© 2014. Published by The Company of Biologists Ltd | Journal of Cell Science (2014) 127, 2885–2897 doi:10.1242/jcs.145334

RESEARCH ARTICLE

Peptide-independent stabilization of MHC class I molecules breaches cellular quality control

Zeynep Hein[1], Hannes Uchtenhagen[2], Esam Tolba Abualrous[1], Sunil Kumar Saini[1], Linda Janßen[1], Andy Van Hateren[3], Constanze Wiek[4], Helmut Hanenberg[4], Frank Momburg[5], Adnane Achour[2], Tim Elliott[3,*], Sebastian Springer[1,*] and Denise Boulanger[3]

ABSTRACT

The intracellular trafficking of major histocompatibility complex class I (MHC-I) proteins is directed by three quality control mechanisms that test for their structural integrity, which is correlated to the binding of high-affinity antigenic peptide ligands. To investigate which molecular features of MHC-I these quality control mechanisms detect, we have followed the hypothesis that suboptimally loaded MHC-I molecules are characterized by their conformational mobility in the F-pocket region of the peptide-binding site. We have created a novel variant of an MHC-I protein, K^b-Y84C, in which two α-helices in this region are linked by a disulfide bond that mimics the conformational and dynamic effects of bound high-affinity peptide. K^b-Y84C shows a remarkable increase in the binding affinity to its light chain, beta-2 microglobulin (β_2m), and bypasses all three cellular quality control steps. Our data demonstrate (1) that coupling between peptide and β_2m binding to the MHC-I heavy chain is mediated by conformational dynamics; (2) that the folded conformation of MHC-I, supported by β_2m, plays a decisive role in passing the ER-to-cell-surface transport quality controls; and (3) that β_2m association is also tested by the cell surface quality control that leads to MHC-I endocytosis.

KEY WORDS: Antigen presentation, Endocytosis, Major histocompatibility complex, ER quality control

INTRODUCTION

The correct assembly of major histocompatibility complex class I (MHC-I) molecules that are bound to peptide ligands with high affinity (hereafter, high-affinity peptides) is supported by chaperone proteins and monitored at several stations of the secretory pathway to warrant efficient cellular immune responses against pathogens and tumors.

The first quality control step takes place in the endoplasmic reticulum (ER). After their cotranslational insertion into the ER membrane, the lumenal domains of MHC-I heavy chains are first bound by the lectin chaperone calnexin and the disulfide isomerase ERp57 (also known as PDIA3). Then, they bind to the light chain, β2-microglobulin (β_2m). Heterodimers between MHC-I heavy chain and β_2m associate with the lectin chaperone calreticulin and a pre-existing complex of the transporter associated with antigen processing (TAP), the TAP-associated protein tapasin and the ERp57, forming together the peptide loading complex (PLC). Prior to loading with high-affinity peptides, suboptimally loaded MHC-I molecules are usually bound to the PLC and are retained in the ER owing to the KKxx sequence that is present on the cytosolic tail of tapasin (Paulsson et al., 2006). As soon as they are loaded with peptides at sufficient affinity, the trimers of MHC-I heavy chain, β_2m and peptide dissociate from the PLC and exit the ER.

The second quality control step occurs at the border between the cis- and medial Golgi. MHC-I molecules are again monitored for high-affinity peptide occupancy by a system that is related to the standard glycoprotein quality control (Ellgaard and Helenius, 2001). It recognizes suboptimally loaded MHC-I, most likely through UDP-glucose:glycoprotein glucosyltransferase (UGT1), retains them in the ER-Golgi intermediate compartment (ERGIC) and the cis-Golgi, prevents them from becoming endoglycosidase H resistant, and eventually returns them to the ER with the help of calreticulin (Hsu et al., 1991; Paulsson et al., 2006; Garstka et al., 2007; Purcell and Elliott, 2008; Wearsch and Cresswell, 2008; Howe et al., 2009; Zhang et al., 2011). This second system is responsible for the intracellular retention of tapasin-dependent MHC-I allotypes in tapasin-deficient cells (Peh et al., 1998; Garstka et al., 2011).

Third, after some time at the cell surface, MHC-I lose their peptide ligand and β_2m, and the resulting free heavy chains are transported to lysosomes for proteolytic destruction (Mahmutefendić et al., 2011). The molecular mechanisms of this surface quality control process and its exact location in the endocytic branch of the secretory pathway are not well understood.

The molecular properties of suboptimally loaded MHC-I that are recognized by these three quality control systems are poorly characterized because crystal or nuclear magnetic resonance structures of empty MHC-I molecules are still not available. Suboptimally loaded MHC-I have a decreased affinity to β_2m, lower thermal stability, a larger hydrodynamic radius and greater conformational mobility of individual residues compared to high-affinity peptide-bound MHC-I (Elliott et al., 1991; Fahnestock et al., 1992; Springer et al., 1998; Mage et al., 2012; Kurimoto et al., 2013); thus, suboptimally loaded MHC-I molecules have been compared to molten globules (Bouvier and Wiley, 1998; Saini et al., 2013). In support of this view, comparative molecular

[1]Molecular Life Science Center, Jacobs University Bremen, 28759 Bremen, Germany. [2]Science for Life Laboratory, Department of Medicine Solna, Karolinska Institutet, SE-171 77 Stockholm, Sweden. [3]Cancer Sciences Unit, Faculty of Medicine, University of Southampton, Southampton, Hampshire SO16 6YD, UK. [4]Department of Otorhinolaryngology, Heinrich-Heine-University Düsseldorf, 40225 Düsseldorf, Germany. [5]Division of Translational Immunology, German Cancer Research Center, 69120 Heidelberg, Germany.

*Authors for correspondence (sebastian.springer@queens.oxon.org; T.J.Elliott@soton.ac.uk)

Received 26 October 2013; Accepted 15 April 2014

Journal of Cell Science

Journal of Cell Science (2014) 127, 2885–2897 doi:10.1242/jcs.145334

dynamics simulations on empty and peptide-bound murine and human MHC-I have indicated a substantially increased mobility of peptide-empty MHC-I, especially in those parts of the α_1 and α_2 helices that delineate the F-pocket (Sieker et al., 2007; Sieker et al., 2008). Intriguingly, mobility of the polypeptide backbone and related features, such as exposed hydrophobic patches, are recognized by UGT1 (Ruddock and Molinari, 2006). Based on these data, we have proposed that the increased mobility of empty and suboptimally loaded MHC-I, as well as other derived features, are recognized by the cellular quality control mechanisms (Wright et al., 2004; Van Hateren et al., 2010).

Here, we have tested this hypothesis by designing a novel variant of the murine MHC-I allotype H-2K^b, in which the α_1 and α_2 helices are connected by a disulfide bond close to the F-pocket, restricting their mobility. The C84–C139 disulfide bond allows normal PLC interaction and antigen presentation but renders MHC-I surface expression TAP- and tapasin-independent, accelerates anterograde transport, and greatly decreases the rate of MHC-I endocytosis. We demonstrate that these phenotypes can be mostly explained by the increased affinity of the variant K^b protein for β_2m. Our results reveal (1) that the immobilization of the MHC-I polypeptide backbone by the peptide ligand allows MHC-I to pass all three known cellular quality control steps, (2) that peptide binding and β_2m binding to MHC-I are coupled to each other through the molecular dynamics of MHC-I, and (3) that the quality control processes in the ER and Golgi act on several different forms of MHC-I that are linked by dynamic equilibria.

RESULTS

Introduction of a disulfide bond between the α_1 and α_2 helices restricts the flexibility of the F-pocket region

To understand how cells differentiate between MHC-I molecules that are bound to high-affinity peptides and suboptimally loaded MHC-I molecules (i.e. MHC-I with low-affinity peptides or without any peptide), we first wished to identify potential molecular differences between these forms by computer simulation. Previously published molecular dynamics simulations of the α_1 and α_2 domain or of entire MHC-I have suggested one eminent difference between empty and peptide-bound MHC-I: in the absence of peptide, the helical sections that flank the F-pocket region (residues 74–85 and 138–149 in the α_1 and α_2 helices, respectively) were significantly more mobile (Zacharias and Springer, 2004; Garstka et al., 2011; Narzi et al., 2012). Indeed, the corresponding region of peptide-empty HLA-B*07:01 is highly susceptible to proteases (Bouvier and Wiley, 1998), suggesting partial unfolding on a longer time scale. We therefore hypothesized that bound peptides restrict the mobility of this region, and that a similar conformational restriction might be achieved by linking the α_1 and α_2 helices with a disulfide bond. Molecular modeling indicated that the distance between residues 139 and 84 was suitable for the formation of a disulfide bond between two cysteine residues (Fig. 1A). In agreement with our hypothesis, molecular dynamics simulations of the peptide-binding domain of the resulting protein, H-2K^b(A139C/Y84C) (hereafter called K^b-Y84C), indicated a strong restraint of the distance between the alpha carbon atoms of C84 and C139 compared to wild-type K^b (visible as a small variance, i.e. fluctuation, of the distance in Fig. 1B, left). This restraint affected the entire F-pocket region [seen as blue (low-mobility pairwise distances) in Fig. 1C and supplementary material Fig. S1B], but weakened after three helical turns, between residues 73 and 150 (Fig. 1B, right). Interestingly, the absolute mobility of the backbone of empty K^b-Y84C was similar to that of K^b in complex with a high-affinity peptide (Fig. 1D, color-coded root mean square fluctuations of the individual residues over the course of the simulation). Taken together, the molecular dynamics simulation data suggest that the effect of the C84–C139 disulfide bond in K^b-Y84C mimics the effect of the bound peptide on the conformational dynamics of wild-type MHC-I.

Recombinant K^b-Y84C binds peptide efficiently and is highly thermostable

Next, we tested whether K^b-Y84C was able to bind peptides. The ER-lumenal domains of K^b-Y84C and wild-type K^b were produced in *E. coli* and folded *in vitro* with human β_2m and the peptides FAPGNYPAL (Sendai virus nucleoprotein residues 324–332; single-letter amino acid code) or SIINFEKL (ovalbumin residues 257–264). These complexes were then subjected to thermal denaturation monitored by tryptophan fluorescence (TDTF) (Springer et al., 1998; Saini et al., 2013) to assess their structural stability (Morgan et al., 1997) (Fig. 1E). The denaturation temperature (corresponding to the midpoint of transition, T_m) of K^b-Y84C was only slightly lower than that of wild-type K^b, suggesting that peptide-bound K^b-Y84C was nearly as stable as wild-type K^b. In contrast, peptide-free K^b-Y84C (Saini et al., 2013) was significantly more thermostable than wild-type K^b (Fig. 1E, lower panel). The same was true for K^b-Y84C in complex with the C-terminally truncated peptide variants SIINFEK and FAPGNYP-NH$_2$ (with its C terminus amidated). The thermal denaturation of K^b and K^b-Y84C in complex with AVYNFATM [the K^b-restricted lymphocytic choriomeningitis virus (LCMV)-derived epitope gp34 (Achour et al., 2002)] was also monitored by circular dichroism, revealing that K^b-Y84C–gp34 was less thermostable than K^b–gp34, whereas K^b-Y84C–/AVYNFA was more stable than K^b–AVYNFA (supplementary material Fig. S1D). Thus, in the empty or suboptimally loaded state, K^b-Y84C is more resistant to thermal denaturation than wild-type K^b.

Next, to compare the rates of association of a high-affinity peptide to K^b-Y84C and wild-type K^b, both heavy chains were folded in the absence of peptides (Saini et al., 2013). The peptide SIINFEK$_{TAMRA}$L, which was labeled with the fluorescent dye carboxytetramethylrhodamine (TAMRA) on the side chain of the lysine residue, so as not to interfere with binding to K^b, was added, and binding kinetics were measured by fluorescence anisotropy (Fig. 1F). The binding to K^b-Y84C was considerably faster than to wild-type K^b, suggesting that peptide-empty K^b-Y84C is more amenable to peptide binding. Dissociation of SIINFEK$_{TAMRA}$L from K^b-Y84C was slightly faster than K^b (Fig. 1G), in accordance with the slightly lower thermostability of K^b-Y84C shown in Fig. 1E.

The crystal structure of the K^b-Y84C–gp34 complex was determined to 2.1 Å resolution (Fig. 2; supplementary material Tables S1, S2), revealing a very similar overall fold to the previously determined crystal structure of wild-type K^b with the same peptide (Velloso et al., 2004). Importantly, the conformation of the gp34 peptide is very similar in both complexes (Fig. 2B,D). The disulfide bond between residues C84 and C139 of K^b-Y84C–gp34 is clearly indicated by the electron density (Fig. 2C, right panel). The side chain of residue Y84, which plays a key role in the tethering of the C terminus of the peptide in wild-type K^b, is replaced in K^b-Y84C by two water molecules that link the C-terminal carboxylate of the peptide to

Journal of Cell Science (2014) 127, 2885–2897 doi:10.1242/jcs.145334

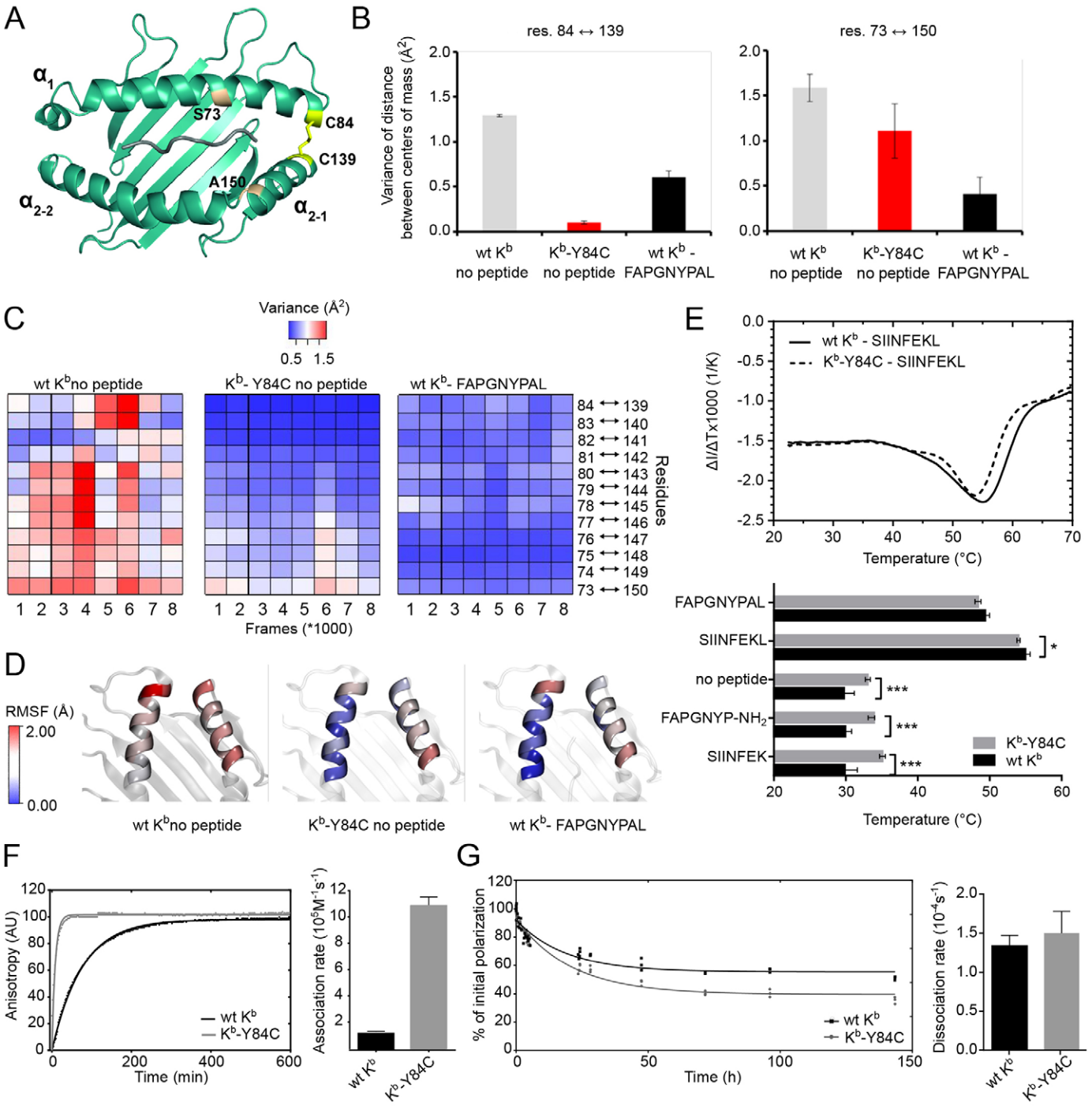

Fig. 1. See next page for legend.

residues Y123 and K146 of the heavy chain through a network of hydrogen bonds (Fig. 2C, left panel). In conclusion, our data demonstrate that K^b-Y84C binds peptides, and that the three-dimensional structure of K^b-Y84C–gp34 is very similar to K^b–gp34.

K^b-Y84C binds and presents endogenous peptides

We next asked whether K^b-Y84C functions in antigen presentation similarly to the wild-type K^b. We introduced GFP fusions of the full-length K^b-Y84C-encoding gene into BL/6 and 3T3 mouse fibroblasts as well as into HeLa cells. Indeed, the K^b-Y84C protein formed the additional C84–C139 disulfide bond because it migrated faster than wild-type K^b in non-reducing denaturing SDS-PAGE of immunoprecipitates from cell lysates, indicating a more compact state (supplementary material Fig. S1E). The surface levels of K^b-Y84C–GFP (detected by their N-terminal HA tag and analyzed in a dosage-dependent manner that is explained in supplementary material Fig. S1F,G) were comparable to K^b–GFP in murine cells, but significantly higher in HeLa (Fig. 3A, top row). In microscopy, both K^b–GFP and

Journal of Cell Science (2014) 127, 2885–2897 doi:10.1242/jcs.145334

Fig. 1. Locally restricted molecular dynamics and peptide binding of K^b-Y84C. (A) Two cysteine residues at positions 84 and 139 of H-2K^b can form a disulfide bond in this model picture. Residues S73 and A150 (see Fig. 1B) are also labeled. (B) The C84–C139 disulfide bond restricts the movement of the polypeptide backbone of K^b-Y84C but only in its direct vicinity. Variance of the distance between the α-carbons of residues 84 and 139 (left) and residues 73 and 150 (right) over the course of a 32-ns molecular dynamics simulation (following 8 ns of equilibration). The positions of residues 73 and 150 in the crystal structure are indicated in Fig. 1A. The overall RMSD chart for the simulation is shown in supplementary material Fig. S1A. (C) The molecular dynamics of K^b-Y84C in its empty state resembles that of wild-type K^b with peptide bound more closely than that of empty wild-type K^b. For each simulation, squares show the color-coded variance over 1000 consecutive frames per square for the distance between the Cα atoms of residues opposing each other across the peptide-binding groove. Total length of the simulation was 40 ns (8 squares). (D) In the vicinity of the C84–C139 disulfide bond, the dynamics of the empty K^b-Y84C equals that of peptide-bound wild-type K^b. Color-coded structure based on the root mean square fluctuation (RMSF) values of the α-carbons of indicated residues. The RMSF chart is shown in supplementary material Fig. S1C. (E) Stability of K^b–peptide complexes determined by TDTF (thermal denaturation measured by tryptophan fluorescence). Complexes of K^b–β_2m with the indicated peptides were subjected to heat denaturation, and fluorescence of endogenous tryptophan residues was recorded. Top panel, LOWESS fit of the first derivative of the fluorescence curve. The transition midpoint (melting temperature, T_m) is determined from the minimum of the curve. Bottom panel, T_m values for different complexes (mean±s.e.m.; n=7, 7, 7, 7, 9, 9, 11, 11, 4, 4 from top to bottom). (F) Peptide binds faster to K^b-Y84C than to wild-type K^b. Left, wild-type K^b and K^b-Y84C were folded empty, 100 nM SIINFEK$_{TAMRA}$L was added and anisotropy of the peptide was followed over time. The line is a first-order one-step on-rate fit. Right, averages of on-rate fits from five measurements (from three independent experiments) (mean±s.e.m.). (G) Peptide dissociates faster from K^b-Y84C. Wild-type K^b and K^b-Y84C were folded with SIINFEK$_{TAMRA}$L peptide. Excess unlabeled SIINFEKL peptide was added, and peptide dissociation was followed by fluorescence polarization at room temperature. wt, wild-type.

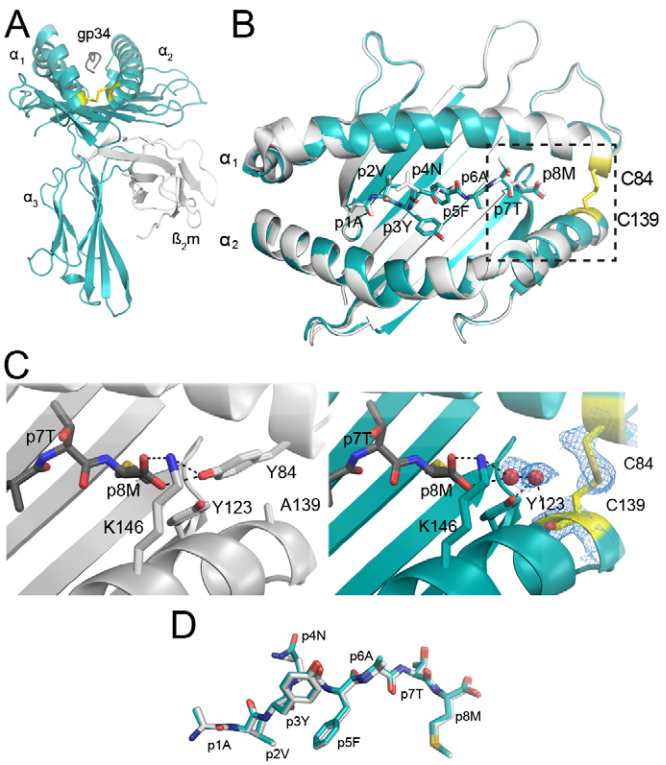

Fig. 2. The crystal structure of K^b-Y84C reveals high structural similarity to the wild-type molecule. (A) View of the K^b-Y84C in complex with AVYNFATM peptide. The C84–C139 disulfide bond is highlighted in yellow. (B) Superimposed wild-type K^b (gray) and K^b-Y84C (cyan) mutant structures reveal identical architecture of the peptide-binding groove and the peptide. The α3 domain and β_2m are omitted from the visualization. (C) Binding of the peptide C-terminus in wild-type K^b (left) and in K^b-Y84C (right). The gap in K^b-Y84C resulting from the absence of the side chain of Y84 is occupied by two water molecules (red), which are held in place by interactions with Y123, K146 and C139. (D) Kb-Y84C binds peptide in the same fashion as wild-type K^b. Overlay of the AVYNFATM peptide in the binding grooves of wild-type K^b (gray) and K^b-Y84C (cyan) shows that the positioning of the backbone of the peptide is conserved in the disulfide mutant with a minor shift towards the α_1 helix.

K^b-Y84C–GFP in BL/6 fibroblasts displayed strong ER and surface stain (supplementary material Fig. S2A).

To investigate whether K^b-Y84C can bind endogenous peptides and present them at the cell surface, we transfected 3T3 fibroblasts and HeLa cells with either wild-type K^b–GFP or K^b-Y84C–GFP and with plasmids encoding the peptide MSIINFEKL (pCyto-SIINFEKL). The K^b–SIINFEKL complexes were monitored at the cell surface using the monoclonal antibody (mAb) 25-D1.16, which specifically recognizes the K^b–SIINFEKL complex (Porgador et al., 1997; Mareeva et al., 2008). K^b-Y84C–SIINFEKL complexes were detected at the cell surface in amounts that were slightly lower than those of wild-type K^b–SIINFEKL (Fig. 3A, center row). We therefore considered the possibility that K^b-Y84C might be less efficient in presenting the SIINFEKL peptide, and we plotted the ratio of the 25-D1.16 over HA signals against the heavy chain expression level (Fig. 3A, bottom row). Intriguingly, the 25-D1.16:HA ratio was higher for wild-type K^b than for K^b-Y84C, which suggests that K^b-Y84C is indeed less efficient in presenting the SIINFEKL peptide. Given that productive interaction with tapasin enables K^b to select SIINFEKL from a large excess of low-affinity peptide (Praveen et al., 2010), it appears that K^b-Y84C, although more stable in its empty form, is slightly compromised in binding to tapasin and/or functionally interacting with it.

We next asked whether K^b-Y84C can present bound peptides to T cells, and therefore we introduced the GFP fusion genes into HeLa cells by transfection together with plasmids encoding the peptide SIINFEKL targeted either to the cytosol (pCyto-SIINFEKL) or to the ER (pER-SIINFEKL, with a preceding signal sequence). We then incubated the cells with the B3Z hybridoma cells, which specifically recognize the K^b–SIINFEKL complex (Karttunen et al., 1992), and monitored the activation of B3Z cells by measuring β-galactosidase activity. K^b-Y84C and wild-type K^b were equal in their ability to present endogenous SIINFEKL to B3Z cells (Fig. 3B). Intriguingly, when murine Ltk^- cells expressing K^b-Y84C were incubated with increasing amounts of exogenous SIINFEKL peptide before exposure to B3Z cells, B3Z cell activation was much stronger for K^b-Y84C than for wild-type K^b (supplementary material Fig. S2B).

Taken together, our data demonstrate that K^b-Y84C efficiently acquires and presents intracellular peptides, and that it presents exogenous peptides to T cells more efficiently than wild-type K^b.

K^b-Y84C surface expression is independent of TAP and tapasin

For efficient expression at the cell surface, most MHC-I allotypes require peptide supply to the ER (mediated by the TAP transporter) and molecular chaperoning by tapasin (Van Kaer et al., 1992; Grandea et al., 2000). To assess whether the surface expression of K^b-Y84C required TAP and tapasin, we

Journal of Cell Science (2014) 127, 2885–2897 doi:10.1242/jcs.145334

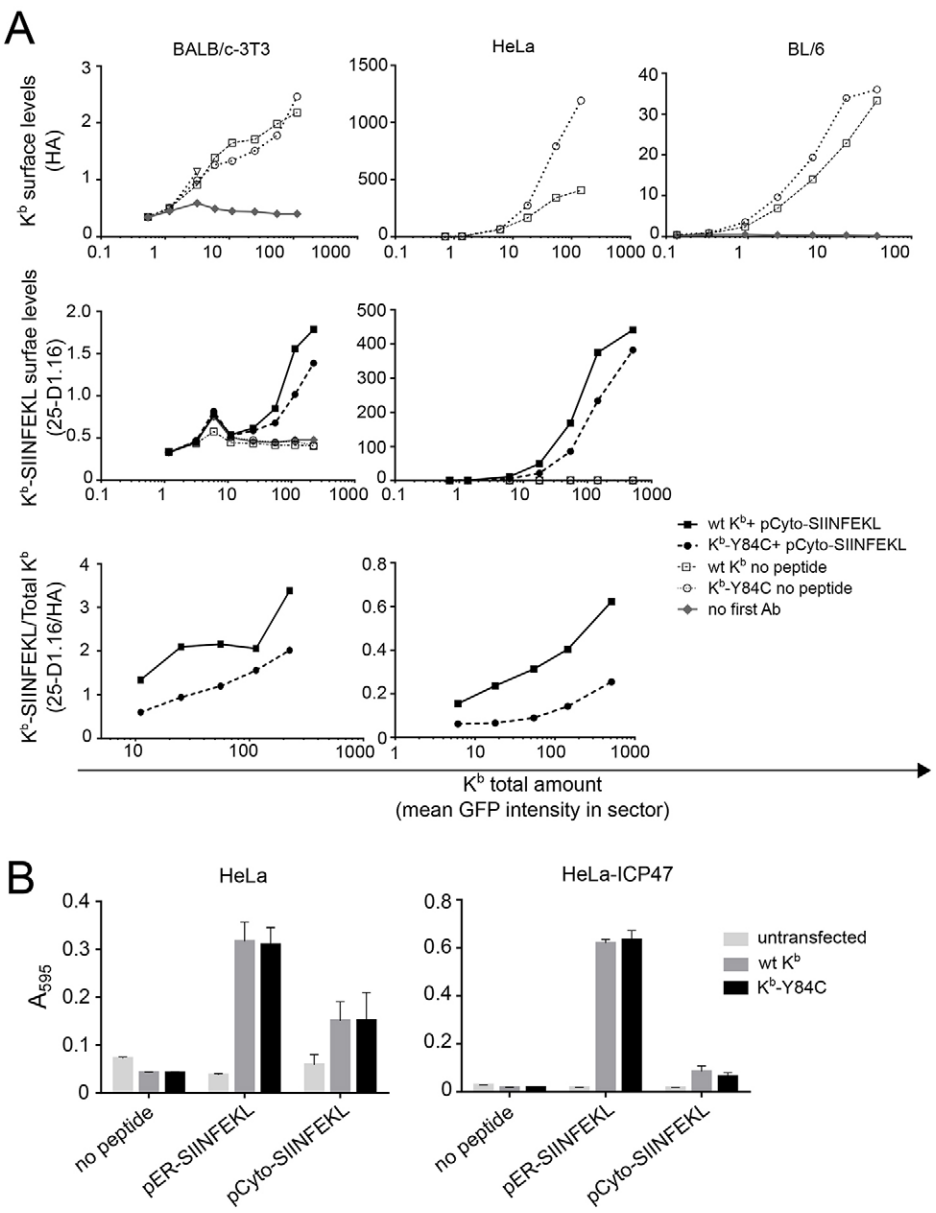

Fig. 3. K^b-Y84C is transported to the cell surface, binds endogenous peptides, and activates T cells. (A) Analysis of K^b surface expression and presentation of the SIINFEKL peptide on HeLa cells (center) and on two murine fibroblast cell lines (BL/6 and BALB/c-3T3). Top row, total surface expression. Cells were transiently transfected with N-terminally HA-tagged K^b heavy chains fused to GFP at their C terminus. Total surface K^b molecules were detected by flow cytometry using anti-HA mAb. For the quantification, mean intensities of anti-HA and GFP fluorescence were determined in eight separate vertical sectors (see supplementary material Fig. S1G). Center row, presentation of the SIINFEKL peptide. Cells were transiently transfected with the same constructs as above. A plasmid expressing the MSIINFEKL peptide in the cytosol (pCyto-SIINFEKL) was co-transfected. Surface K^b–SIINFEKL complexes were detected by mAb 25 D1.16. The total amount of K^b at the cell surface was detected by anti-HA mAb. Controls are no first antibody and no transfected peptide. Bottom row, efficiency of peptide presentation in 3T3 and HeLa cells is displayed as the ratio of 25-D1.16 signal over HA. (The HA values used for the calculation are from the experiments in the center row, and are not shown here). (B) Presentation of SIINFEKL peptides targeted to the cytosol and to the ER. HeLa wild-type cells (left panel) and HeLa cells stably expressing the TAP inhibitor peptide ICP47 (right panel) were transiently co-transfected with K^b–GFP constructs and either cytosolic MSIINFEKL (pCyto-SIINFEKL) or SIINFEKL preceded by a ER-targeting signal (pER-SIINFEKL). Cells were co-cultured with the K^b-SIINFEKL-reactive T cell hybridoma, B3Z, and T cell activity was measured by β-galactosidase colorimetry. wt, wild-type.

investigated its surface levels by flow cytometry in transfected TAP- and tapasin-deficient mouse fibroblasts. Strikingly, surface expression of K^b-Y84C was far higher than that of wild-type K^b (Fig. 4A). This was true for detection both with the antibody specific to the HA epitope tag, with which the K^b proteins were tagged at their N termini, and with the Y3 antibody, which recognizes a β_2m-dependent conformational epitope on the α_1 and α_2 helices of K^b (Hämmerling et al., 1982). In agreement with the flow cytometry results, strong surface expression of K^b-Y84C, but not of wild-type K^b, was observed in immunofluorescence microscopy analyses of TAP- and tapasin-deficient cells with anti-HA antibodies (Fig. 4B). Therefore, in contrast to wild-type K^b, K^b-Y84C can traffic to the cell surface and maintain a steady-state presence there even if peptide or tapasin are unavailable.

K^b-Y84C functionally interacts with the PLC in wild-type cells

To assess whether the TAP and tapasin independence were due to a general inability of K^b-Y84C to interact with the PLC, we next performed co-immunoprecipitation experiments with K^b-Y84C and wild-type K^b in HeLa cells. Both coprecipitated efficiently with TAP and tapasin (Fig. 5A). To test the functionality of this interaction, we used a previously characterized set of variants of the SIINFEKL peptide (SIINFEKM, SIINFEKV, SIINFEKI and SIINYEKL). Their relative surface presentation efficiencies depend on the editing of the peptide repertoire by tapasin (Howarth et al., 2004). We introduced K^b-Y84C or wild-type K^b into HeLa cells, together with plasmids encoding the SIINFEKL variants, and quantified their surface presentation by flow cytometry with mAb 25-D1.16. The presentation hierarchies for K^b-Y84C and wild-type K^b were similar, which suggests that tapasin acts in a similar fashion on both proteins (Fig. 5B). Taken together, these results show that K^b-Y84C is able to interact with tapasin and the PLC, but is not dependent on these interactions for steady-state surface expression.

Faster anterograde transport of K^b-Y84C

The stronger steady-state expression of K^b-Y84C at the cell surface compared to wild-type K^b in the absence of TAP or

Journal of Cell Science (2014) 127, 2885–2897 doi:10.1242/jcs.145334

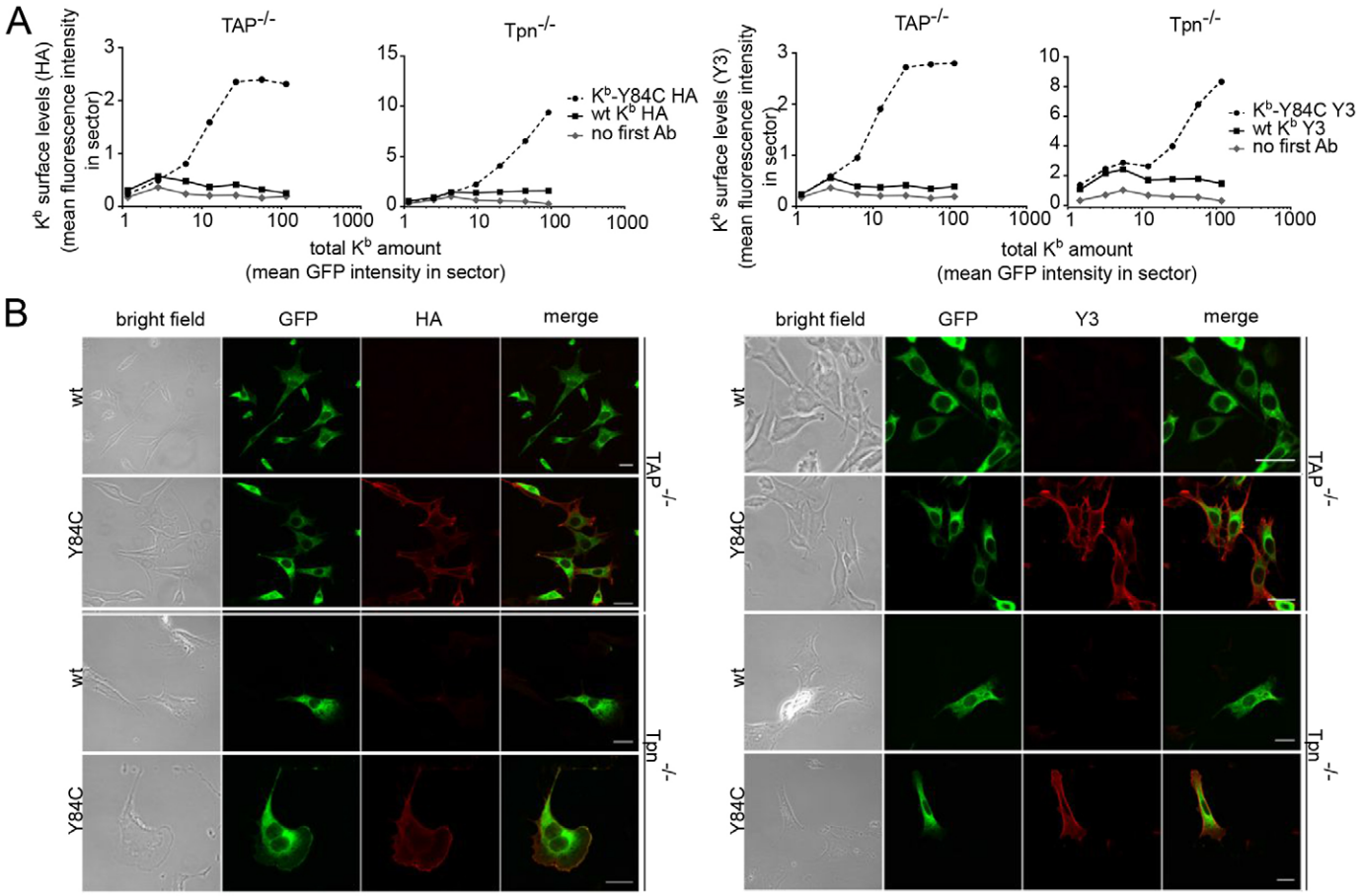

Fig. 4. K^b-Y84C does not require TAP or tapasin for surface transport. (A) Surface expression by flow cytometry. TAP- and tapasin-deficient BL/6 fibroblasts were transiently transfected with HA–K^b–GFP constructs, and the amount of K^b molecules was measured at the cell surface by anti-HA (left panel) and conformation-specific Y3 antibody (right panel). Quantitative analysis was performed as described in supplementary material Fig. S1G. (B) Surface expression by fluorescence microscopy. TAP- and tapasin-deficient BL/6 fibroblasts were transfected with HA–K^b–GFP constructs and stained with anti-HA antibody without permeabilization (left panel). GFP fusion proteins (green) are distributed throughout the secretory pathway and excluded from nuclei and cytoplasm. Surface localization (anti-HA antibody, left panel; Y3, right panel) can only be detected for K^b-Y84C but not for wild-type K^b. In tapasin-deficient cells, low levels of Y3 signal are detected in all cells. The signal of transfected wild-type K^b at the cell surface does not exceed background Y3 levels in these cells, whereas a strong staining of K^b-Y84C at the surface is seen. wt, wild-type. Scale bars: 20 μm.

tapasin could be the result of a more efficient anterograde transport of K^b-Y84C, a decreased rate of endocytic destruction of K^b-Y84C, or both. To investigate the first possibility, we compared the rates of anterograde transport of K^b-Y84C and wild-type K^b in a pulse–chase experiment. [To prevent internalization and degradation of any K^b molecules that reached the cell surface, we added the peptide SIINFEKL to the medium; this treatment does not significantly promote anterograde transport of MHC-I from the cell interior (Townsend et al., 1989)]. In the initial time points of the chase

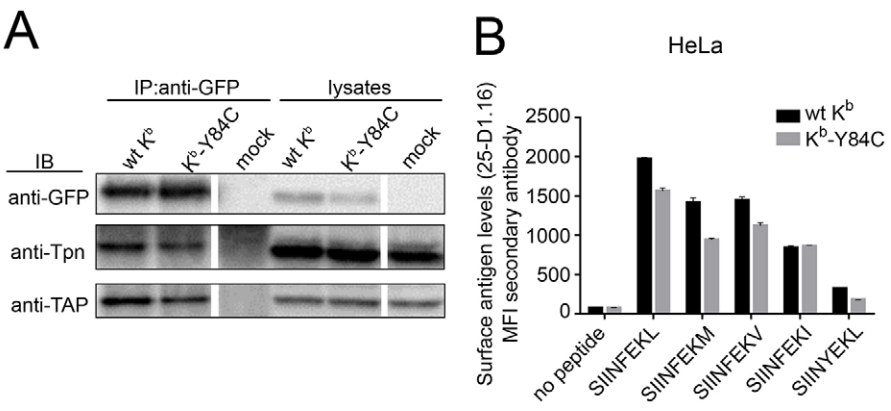

Fig. 5. K^b-Y84C interacts with the PLC. (A) HeLa cells were transfected with K^b–GFP constructs, and protein complexes were precipitated with anti-GFP antibody in digitonin lysates. Immuno-isolates were resolved on SDS-PAGE and transferred onto nitrocellulose membranes by electroblotting. Co-immunoprecipitated proteins were detected by incubating the membranes with antibodies against TAP and tapasin. Corresponding lysates were tested as controls (three wells on the right). (B) Variants of MSIINFEKL peptide were co-expressed with K^b–GFP in HeLa cells. The abundance of K^b–peptide complexes at the cell surface was measured by staining with mAb 25 D1.16 and flow cytometry. wt, wild-type.

Journal of Cell Science (2014) 127, 2885–2897 doi:10.1242/jcs.145334

in wild-type cells, K^b-Y84C traveled only slightly faster than wild-type K^b (Fig. 6A, top panel; Fig. 6B, left). In contrast, there was a substantial difference between the K^b proteins in TAP- and in tapasin-deficient cells, where wild-type K^b was mostly restricted to the ER, whereas K^b-Y84C was eventually transported to the cell surface (Fig. 6A, center and bottom panels; Fig. 6B, center and right).

In conclusion, our data suggest that the anterograde transport of K^b-Y84C is faster than that of K^b, especially for the suboptimally loaded proteins in TAP- or tapasin-deficient cells.

K^b-Y84C is highly stable at the cell surface and displays increased β_2m affinity

Following peptide dissociation, MHC-I molecules lose β_2m at the cell surface and become internalized and transported to lysosomes, where they are destroyed by proteases (Mahmutefendić et al., 2011). Thus, the second possible reason for the high steady-state expression levels of K^b-Y84C on the surface of TAP- and tapasin-deficient cells (Fig. 4) is slower internalization and/or lysosomal targeting of suboptimally loaded K^b-Y84C after the loss of high-affinity peptide.

To obtain suboptimally loaded K^b proteins on the cell surface, we used HeLa-ICP47 cells [i.e. HeLa cells that were made functionally TAP-deficient by stable transduction with the herpesvirus protein ICP47 (Früh et al., 1995)], which were transfected with K^b-Y84C or wild-type K^b constructs and incubated overnight at 26°C to block endocytosis (Ljunggren et al., 1990; Day et al., 1995). We then performed a brefeldin A (BFA) decay assay in which we shifted the cells to 37°C to induce endocytosis of suboptimally loaded K^b proteins after adding BFA to prevent any surface transport of newly synthesized MHC-I. Surface levels of K^b and K^b-Y84C were measured at different times by mAb Y3 staining and flow cytometry (Fig. 7A). As expected, suboptimally loaded wild-type K^b was endocytosed with a half-life of ~4 h and could be stabilized by addition of the peptide SIINFEKL. In striking contrast, K^b-Y84C was stable at the cell surface even without any added peptide, suggesting that it is resistant to endocytosis even when suboptimally loaded. Our data show that the increased steady-state levels of K^b-Y84C at the surface of TAP- and tapasin-deficient cells are due to a combination of two factors: its more efficient anterograde transport, and the resistance of its suboptimally loaded form to endocytosis.

Given that dissociation of β_2m likely precedes the endocytic destruction of MHC-I (Zagorac et al., 2012), we hypothesized that suboptimally loaded K^b-Y84C is stable at the cell surface because of its higher affinity to β_2m. To test this hypothesis, we immunoprecipitated K^b–GFP complexes from transfected HeLa-ICP47 cells with anti-GFP antibody and followed the dissociation of β_2m from the heavy chain over time at 37°C (Fig. 7B). Indeed, β_2m dissociated much faster from wild-type K^b than from K^b-Y84C, suggesting that it binds more tightly to the K^b-Y84C heavy chain. Likewise, decreasing levels of β_2m bound to the heavy chain over time were seen for wild-type K^b but not for K^b-Y84C in pulse–chase experiments in TAP-deficient cells (supplementary material Fig. S2C,D).

Given that K^b-Y84C has a higher affinity to β_2m, it is expected to associate more efficiently with β_2m under conditions where β_2m is limiting. To test whether this phenomenon explains the faster surface transport of K^b-Y84C that we observed in TAP- and tapasin-deficient cells, we performed a pulse–chase analysis similar to Fig. 6, but this time we simultaneously overexpressed β_2m. Interestingly, the rate of acquisition of resistance to EndoF1 was essentially identical for wild-type K^b and K^b-Y84C and much faster than in the absence of β_2m overexpression (Fig. 7C,D). Thus, we conclude that the higher affinity of K^b-Y84C to β_2m is sufficient to explain its faster anterograde transport in tapasin-deficient cells.

We next investigated whether the accelerated transport of wild-type K^b upon β_2m overexpression also decreases the efficiency with which wild-type K^b presents SIINFEKL, in analogy to the lower presentation efficiency of K^b-Y84C (see Fig. 3A). The experiment showed this to be the case (supplementary material Fig. S2E), suggesting that the antigen presentation phenotypes of K^b-Y84C can also be explained by its increased β_2m affinity.

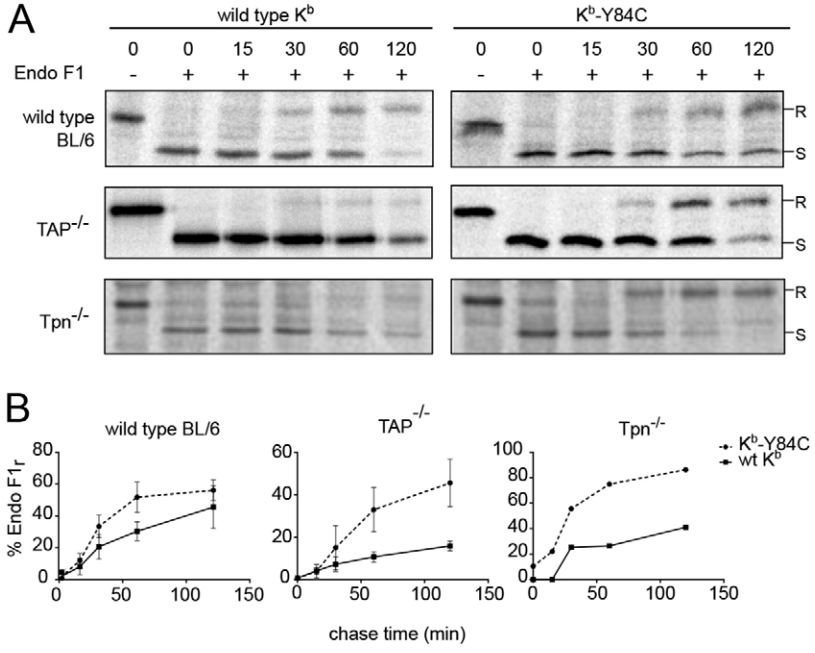

Fig. 6. K^b-Y84C overcomes intracellular retention in PLC-deficient cells. (A) Pulse–chase experiment. N-terminally HA-tagged wild-type K^b and K^b-Y84C were stably expressed by lentiviruses in wild-type and TAP- or tapasin-deficient BL/6 fibroblasts. Newly synthesized proteins were pulse labeled with [35S] methionine/cysteine for 10 min and chased in the presence of non-labeled methionine and cysteine for the indicated times. To prevent endocytosis and subsequent degradation of empty K^b molecules at the surface of TAP- and tapasin-deficient cells, SIINFEKL peptide was added (10 μM final concentration) to the cells during the chase. The immunoisolates were left untreated or digested with Endoglycosidase F1 (EndoF1, see Materials and Methods) where indicated. Samples were resolved on 12% SDS-polyacrylamide gels. In wild-type cells, both K^b-Y84C and wild-type protein matured with similar kinetics, whereas in TAP- and tapasin-deficient cells, K^b-Y84C can achieve EndoF1 resistance at a much higher rate than the wild-type. (B) Quantification of results in A. The EndoF1-resistant population is depicted as the percentage of the total amount of protein at the time points of the chase (mean±s.d., $n \leq 4$; for wild-type and $TAP^{-/-}$ cells). wt, wild-type.

Journal of Cell Science (2014) 127, 2885–2897 doi:10.1242/jcs.145334

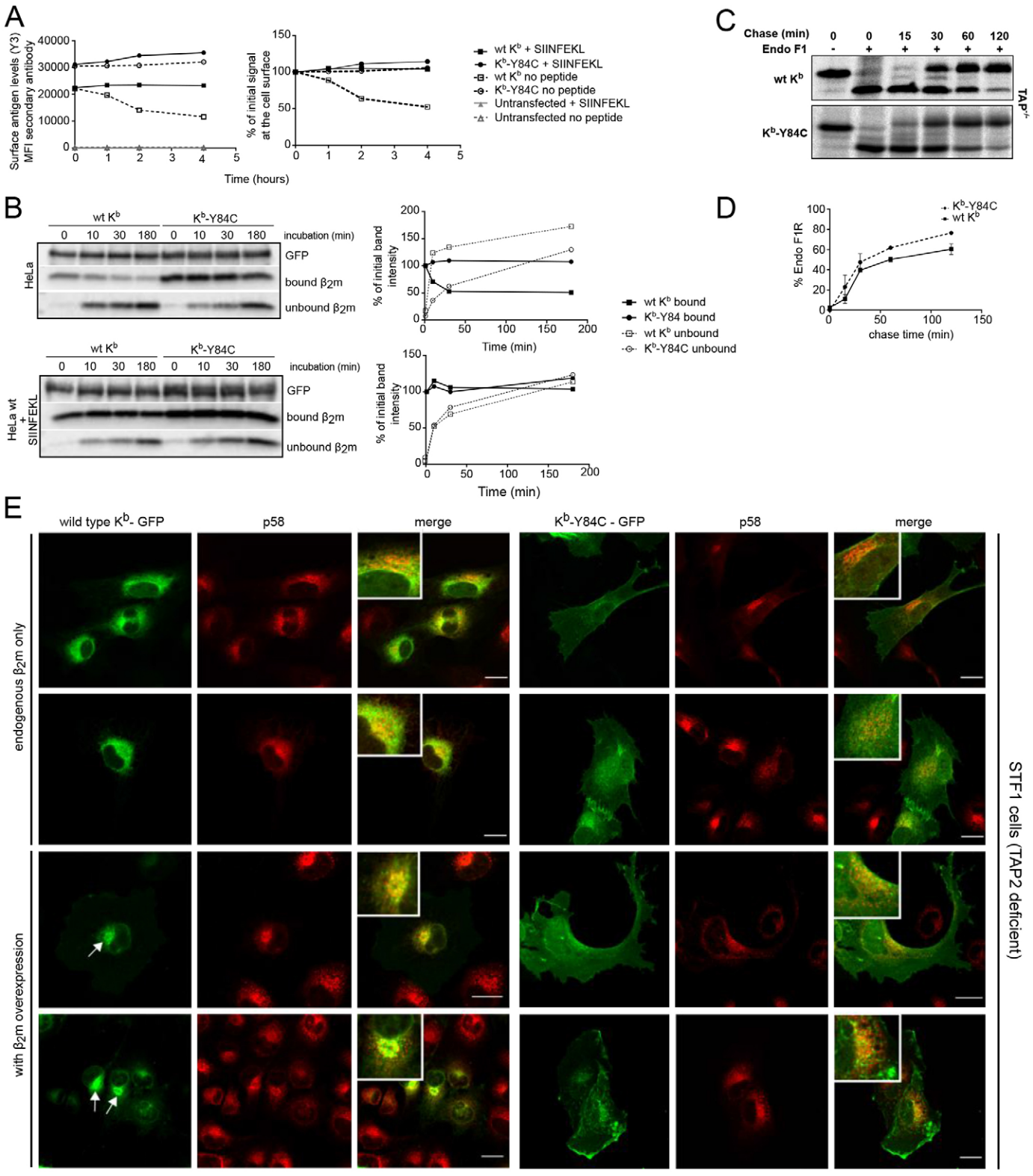

Fig. 7. See next page for legend.

To analyze the trafficking of the K^b proteins in the presence of excess β_2m in more detail, we performed fluorescence microscopy on TAP-deficient cells expressing the C-terminal GFP fusion variants of K^b heavy chains (K^b–GFP). Wild-type K^b–GFP was retained in the ER and showed limited co-localization with the ERGIC marker p58 (also known as LMAN1) (Fig. 7E, top left), whereas K^b-Y84C–GFP was clearly visible at the cell surface and did not appreciably

Journal of Cell Science (2014) 127, 2885–2897 doi:10.1242/jcs.145334

Fig. 7. Suboptimally loaded K^b-Y84C is stable at the cell surface and has an increased affinity to β_2m. (A) Brefeldin A (BFA) decay experiment. K^b–GFP constructs were expressed in HeLa-ICP47 cells. Empty molecules were enriched at the surface by overnight incubation of the cells at 26˚C. Cells were incubated with SIINFEKL peptide or DMSO followed by incubation at 37˚C in the presence of BFA. Left panel, level of K^b complexes at the surface as determined by mAb Y3 antibody. Right panel, the same data normalized to the initial surface levels. (B) Complex dissociation analysis. Left panels, K^b–GFP constructs were expressed in HeLa-ICP47 (top left panel) and wild-type HeLa cells (bottom left panel). Cells were lysed (in the presence of SIINFEKL peptide in the case of wild-type HeLa cells), and K^b protein complexes were immunoprecipitated with anti-GFP antibody and incubated at 37˚C for the indicated times. Proteins remaining on the beads were then resolved by SDS-PAGE and detected with anti-GFP (top sections of panels) for total K^b and anti-β_2m (BBM.1) for detecting K^b-bound β_2m (center sections of panels). The supernatants were also resolved by SDS-PAGE and probed with BBM.1 antibody to detect those β_2m molecules dissociated from the K^b complexes (bottom sections of panels). Right panels: Quantitation of the density of the β_2m bands, normalized to time point zero. (C) TAP deficient BL/6 fibroblasts expressing wild-type K^b or K^b-Y84C from an integrated lentivirus, selected for high expression, were superinfected with a second lentivirus carrying the human β_2m gene. Stable cell lines were pulse labeled (10 min) and chased for indicated times in the presence of SIINFEKL peptide (10 μM in chase medium, to prevent endocytic destruction of any K^b molecules that reached the cell surface). K^b molecules were immunoprecipitated with anti-HA antibody, and the immuno-isolates were treated with EndoF1 where indicated. When β_2m is overexpressed, both wild-type and Y84C mutant of K^b acquire EndoF1 resistance with almost identical kinetics. (D) The EndoF1 resistant population was depicted as percentage of the total amount of protein at the time points of the chase (mean ±SD, $n=2$). (E) Human TAP2-deficient fibroblast cells (STF1) were transiently transfected with wild-type K^b–GFP or K^b-Y84C–GFP and β_2m (lower panels only). Cells were permeabilized and stained with a monoclonal antibody against ERGIC marker p58 (anti-ERGIC-53, red). Surface K^b molecules were not trapped with peptide as in Fig. 7C. wt, wild-type. Scale bars: 20 μm.

colocalize with p58 (Fig. 7E, top right). When we co-expressed β_2m with the K^b heavy chains, we observed that wild-type K^b now exited the ER but accumulated in the p58-positive compartment (Fig. 7E, bottom left, arrows), indicating that it was retained there by the ERGIC and cis-Golgi quality control (Garstka et al., 2007). Small amounts were detected at the cell surface. K^b-Y84C–GFP displayed increased surface levels upon β_2m overexpression, and again no colocalization with the ERGIC marker was observed (Fig. 7E, bottom right). The much weaker surface expression of wild-type K^b upon β_2m overexpression compared to K^b-Y84C–GFP probably reflects the much higher endocytosis rate of wild-type K^b (see Fig. 7A) because, here, we used no peptide in the medium to trap surface class I molecules. Taken together, these results demonstrate that K^b-Y84C is transported to the cell surface rather efficiently, whereas wild-type K^b is at least partially retained in the ERGIC or cis-Golgi, even at increased β_2m levels. This suggests, in accordance to the pulse–chase experiments in Fig. 6, that suboptimally loaded K^b-Y84C can at least partially bypass the Golgi-based quality control that returns suboptimally loaded wild-type K^b to the ER.

DISCUSSION

The novel MHC-I variant described in this study, K^b-Y84C, bypasses all three cellular quality control steps that retain suboptimally peptide-loaded MHC-I molecules in the ER (step 1 as discussed in the Introduction), return them from the *cis*-Golgi to the ER (step 2), or endocytose them from the cell surface for destruction (step 3). We show that this bypass effect is mainly explained by an increased affinity of K^b-Y84C for the light chain, β_2m, and possibly by other effects of the conformational restriction of the F-pocket region by the disulfide bond.

Our molecular dynamics simulations suggest that the effects of the C84–C139 disulfide bond on the conformational dynamics of the K^b heavy chain are similar to the effects of binding a high-affinity peptide. Given that binding of peptide and β_2m to the heavy chain are cooperative (Townsend et al., 1990; Elliott et al., 1991), it is mechanistically consistent that the C84–C139 disulfide bond also increases the β_2m binding affinity of K^b. As we see no significant differences between wild-type K^b and K^b-Y84C in the crystal structure positions of the residues at the interface of the heavy chain with β_2m (Shields et al., 1999; Achour et al., 2002; Achour et al., 2006; Hee et al., 2012), we propose that the coupling between peptide binding and β_2m binding occurs through the conformational dynamics of the heavy chain (Zacharias and Springer, 2004; Beerbaum et al., 2013; Bailey et al., 2014). Further investigation of K^b-Y84C might elucidate this coupling, which is central to MHC-I stability and to the molecular understanding of cellular peptide selection. To analyze conformational dynamics, novel tools are required; as the investigation of heavy-chain–β_2m interactions by nuclear magnetic resonance spectroscopy is only just emerging (Beerbaum et al., 2013; Kurimoto et al., 2013), we think that molecular dynamics analyses with extended simulation times and more refined analytical methods will remain an important tool.

In the cell, we believe that both major phenotypes of K^b-Y84C, namely faster trafficking (i.e. bypass of quality control steps 1 and 2) and increased stability at the cell surface (i.e. bypass of quality control step 3), can be explained by its increased β_2m affinity. At the cell surface, after losing peptide, MHC-I molecules are quickly endocytosed and destroyed. However, the suboptimally loaded form of K^b-Y84C is endocytosed more slowly, probably owing to the reason that it can hold onto β_2m for a longer time. These data support the notion that it is the free heavy chain species of MHC-I that is recognized for rapid transport to lysosomes and proteolytic destruction (Neefjes et al., 1992). Thus, β_2m affinity is a crucial determinant of MHC-I surface levels.

In the forward direction, the overexpression experiments with β_2m (Fig. 7C,D; supplementary material Fig. S2E) show that the more efficient ER-to-surface transport of suboptimally loaded K^b-Y84C (compared to suboptimally loaded wild-type K^b) can be explained by its tighter binding to β_2m. Remarkably, the greater stability of the empty or suboptimally loaded K^b-Y84C–β_2m complex seems to impair its efficient loading with high-affinity peptide, which suggests that its interaction with tapasin is less efficient, perhaps only slightly, concomitant with its faster transport out of the ER.

Our results extend the finding that β_2m is a conformational chaperone for the folding of MHC-I heavy chains (Wang et al., 1994). For the molecular mechanism of this effect, they do not necessarily imply a new mode of β_2m–heavy-chain interaction or a second binding site for β_2m on the heavy chain. More simply, they suggest that the interaction between β_2m and the K^b heavy chain in the ER is close to equilibrium and that in the absence of peptide, β_2m continuously dissociates from and re-associates to the heavy chain, making a certain fraction of the MHC-I pool in the ER unavailable for peptide binding. This interpretation explains how K^b-Y84C, by virtue of its higher β_2m-binding affinity, might bind peptides faster than K^b.

In addition to its increased β_2m affinity, the conformational restriction of the F-pocket region by the C84–C139 disulfide bond

Journal of Cell Science (2014) 127, 2885–2897 doi:10.1242/jcs.145334

might directly help K^b-Y84C to bypass the cis-Golgi quality control. For this, there are two pieces of preliminary evidence. First, when β_2m is overexpressed, suboptimally loaded wild-type K^b still accumulates in the ERGIC and cis-Golgi. We have shown previously that this accumulation is connected to Golgi-to-ER retrieval. In contrast, suboptimally loaded K^b-Y84C barely shows such accumulation (Fig. 7E), suggesting that it is not recognized by the step 2 quality control mechanism (*i.e.* by UGT1). Second, tapasin – in addition to its effect on peptide exchange and optimization (Williams et al., 2002; Chen and Bouvier, 2007; Wearsch and Cresswell, 2007) – helps to structure the peptide-binding site of suboptimally loaded (and thus conformationally disordered) MHC-I molecules, such that they can bind peptide (Kienast et al., 2007; Garstka et al., 2011; Kurimoto et al., 2013). The efficient surface transport of K^b-Y84C in tapasin-deficient cells (Figs 4, 6) might be at least partially caused by the ordering of the F-pocket region by the C84–C139 disulfide bond, which thus substitutes for tapasin. In addition, a stabilizing effect of the increased β_2m affinity might also be at work here.

Fig. 8 shows the simplest model of the cellular assembly of the heavy chain (HC), β_2m, and peptide (P) that is consistent with the data in this paper and elsewhere. It is an extension of the unified qualitative model for peptide binding to MHC-I that we presented previously (Garstka et al., 2011). The model depicts how, in mechanistic terms, the amount of MHC-I available for peptide binding ($HC_{so}\_\beta_2m$ in the model) depends on the β_2m affinity of the heavy chain (K_β), on the amount of β_2m available, and on tapasin dependence (K_S). In this way, we hope that in the future, the differences in the cellular biochemistry of the different MHC-I heavy chain allotypes, which have different β_2m affinities and tapasin dependences, might be explained.

Taken together, our observations show the central role of β_2m in directing the folding and trafficking of MHC-I molecules. Binding of β_2m to the heavy chain is modulated by the bound peptide through conformational and dynamic effects. Much work remains in order to elucidate these fascinating connections on a molecular level.

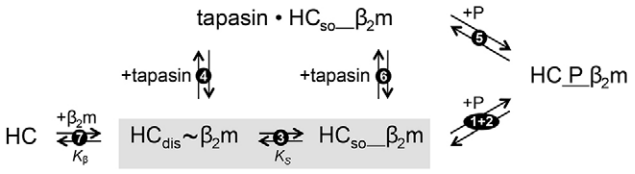

Fig. 8. Unified scheme for the binding of peptide to MHC-I heavy-chain–β_2m heterodimers. Folded MHC-I heavy chains (HC) are in a binding equilibrium with β_2m (reaction 7; equilibrium constant K_β). The HC–β_2m complexes that have not yet bound peptide (gray box) exist in an equilibrium of a disordered ($HC_{dis}\sim\beta_2m$) and a stable open ($HC_{so}\_\beta_2m$; the underscore symbolizes the peptide-receptive binding groove) form (reaction 3). Tapasin-independent MHC-I molecules prefer the stable open form $HC_{so}\_\beta_2m$, to which peptide can bind directly and lead to the stable complex HC P β_2m [reaction 1+2; via the intermediate CP* (Praveen et al., 2010), not shown here]. Tapasin-dependent MHC-I molecules mostly exist in the disordered state $HC_{dis}\sim\beta_2m$, which cannot directly bind peptide. The binding of tapasin (reaction 4) to $HC_{dis}\sim\beta_2m$ allows the binding of peptide (reaction 5). In the absence of tapasin (and thus of reactions 4, 5 and 6), the amount of $HC_{so}\_\beta_2m$ that is available for direct peptide binding depends on the degree of tapasin dependence [K_S, reaction 3 (Garstka et al., 2011)], on the β_2m affinity of the respective allotype (K_β; especially high for K^b-Y84C), and on the β_2m levels in the ER (reaction 7). Figure is modified from figure 5 of Garstka, et al., 2011 to which the reaction numbers correspond.

MATERIALS AND METHODS

Cell lines, reagents and methods using live cells

Wild-type and tapasin-deficient BL/6 mouse fibroblasts (Grandea et al., 2000), TAP-deficient BL/6 mouse fibroblasts (Van Kaer et al., 1992), B3Z hybridoma cells (Karttunen et al., 1992), STF1 and STF1_TAP2 cells (Zimmer et al., 1999) and HeLa ICP47 cells (Edd James, Southampton, UK) were obtained from colleagues. Cells were grown and transfected with DNA using standard protocols. We used monoclonal antibodies 12CA5 (Niman et al., 1983), 25.D1–16 (Porgador et al., 1997), 1–87 (Roder et al., 2009), Y3 and K10–56 (Hämmerling et al., 1982; Arnold et al., 1984) provided by colleagues. Other antibodies were obtained from commercial sources. Radiolabeling and immunoprecipitation were performed as described previously (Fritzsche and Springer, 2013). Immunofluorescence microscopy was performed as described previously (Garstka et al., 2007).

Plasmids and retroviral expression

The A139C and Y84C mutations and the HA epitope tag (YPYDVPDYA) from influenza virus hemagglutinin were sequentially introduced into the wild-type H-2K^b sequence found between the *Sal*I and *Bam*HI sites in pEGFP-N1 (Clontech) by QuikChange site-directed mutagenesis (Agilent). An *Age*I site was introduced into the lentiviral vector puc2CL6IPwo (Halenius et al., 2011) by QuikChange. N-terminally HA-tagged H-2K^b expression constructs (wild-type and A139C/Y84C) were then cloned into this vector via the *Xho*I and *Age*I sites. Lentiviruses were produced and used for gene delivery as described previously (Hanenberg et al., 1996; Moritz et al., 1996; Hanenberg et al., 1997). For cytoplasmic SIINFEKL (residues 257–264 of ovalbumin) expression, the MSIINFEKL sequence was inserted into the pEGFP-N1 by site-directed mutagenesis. pCMVbipep-neo expressing SIINFEKL variant minigenes under the control of the CMV promoter were described previously (Howarth et al., 2004). pER-SIINFEKL and pCyto-SIINFEKL, kind gifts from Edd James, were generated as described previously (Shastri and Gonzalez, 1993; Serwold et al., 2001) using pcDNA3 (Invitrogen).

Antigen presentation assays and FACS analyses

For the T cell activation assay, HeLa wild-type and HeLa ICP47 cells were transfected with the H-2K^b wild-type or Y84C plasmids and pER-SIINFEKL or pCyto-SIINFEKL plasmids. After 2 days, B3Z cells were added and their response quantified as described previously (Sanderson and Shastri, 1994). For Ltk$^-$ cells, transfection and culture was as described previously (Tiwari et al., 2007). For the detection of K^b–SIINFEKL complexes at the cell surface, BALB/c 3T3 or HeLa cells were transiently transfected with plasmids coding for K^b–GFP and SIINFEKL constructs, harvested, stained with mAb 25.D1–16, and counted in a CyFlow Space (Partec) or a FACSCanto (Becton Dickinson). Mean antigen dose and mean antibody staining intensity were calculated as in supplementary material Fig. S1G. For the BFA decay, HeLa ICP47 transfected with wild-type K^b–GFP or K^b-Y84C–GFP were incubated overnight at 26°C and then incubated with 20 µM SIINFEKL peptide or with DMSO for 1 h at 26°C. After washing with medium and adding brefeldin A, cells were transferred to 37°C. At time points as described in the figure legends, cells were trypsinized and stained with Y3 or 25.D1. Data were collected on a FACSCanto (Becton Dickinson).

β_2m dissociation assay

HeLa wild-type and HeLa ICP47 cells transfected with wild-type K^b–GFP or K^b-Y84C–GFP construct were lysed on ice for 30 min in 1% Triton X-100 in water. K^b molecules were immunoprecipitated using anti-GFP rabbit polyclonal antibody bound to Dynabeads–protein-G (Life Technologies). Complexes bound to beads were incubated at 37°C. At time points as described in the figure legends, samples were placed on the magnet to separate the dissociated β_2m from the fraction bound to the heavy chain. Both fractions were separated by SDS-PAGE and transferred onto Hybond C-Extra membranes. Membranes were probed for K^b heavy chain using anti-GFP-HRP rabbit polyclonal antibody and β_2m using an anti-human β_2m rabbit polyclonal antibody (DAKO). Band intensity was quantified using ImageJ (Schneider et al., 2012).

Crystallography

The K^b-Y84C-AVYNFATM complex was produced as described previously (Achour et al., 1999), and folded complexes were purified on Superdex 20 columns (GE Healthcare) and concentrated to 4–7 mg/ml in 20 mM Tris-HCl pH 7.3. Crystallization assays were performed in 24-well plates at 25℃ using the hanging-drop vapor diffusion method. Data collection was performed at beamline ID23-2 at the European Synchrotron Radiation Facility (Grenoble, France). Diffraction data were processed and scaled using the programs MOSFLM 7.0.3 (Leslie, 1992) and SCALA (Evans, 2006). The crystal structure of K^b-Y84C–AVYNFATM was determined by molecular replacement using PHASER (McCoy, 2007) and the crystal structure of wild-type K^b–AVYNFATM (PDB ID: 1S7S) (Velloso et al., 2004), with the peptide omitted, as the search model. A random 5% of the reflections were set aside for monitoring the refinement by R_{free} cross-validation (Brünger, 1992). Refinement was performed using Refmac5 (Murshudov et al., 1997), Phenix.refine (Adams et al., 2010) and Coot (Emsley et al., 2010). Individual atom B factors were refined isotropically and the position of all water molecules, added to the complexes using Coot, was inspected manually. The stereochemistry of the final models was verified using PROCHECK (Laskowski et al., 1993). All figures were created with PyMol (Schrödinger).

Fluorescence anisotropy

Association rate measurements were performed as described previously (Saini et al., 2013). For the dissociation measurements, K^b–β_2m complexes with $SIINFEK_{TAMRA}L$ peptide were incubated with 250 µM unlabeled SIINFEKL peptide at room temperature, and dissociation was followed with a Molecular Devices Analyst AD with excitation at 530 nm and emission at 580 nm and using a 561-nm dichroic mirror.

Molecular dynamics simulations

Molecular dynamics simulations were performed as described previously (Garstka et al., 2011) using the sander module of Amber 9.0 (Case et al., 2005) and the parm03 force field (Duan et al., 2003) with TIP3 water (Jorgensen et al., 1983). starting from 1KPV (Protein Data Bank) and using VMD (Humphrey et al., 1996) for visualization.

The complete Materials and Methods are available from the authors upon request.

Acknowledgements

We would like to thank Malgorzata Garstka (Cell Biology II, Netherlands Cancer Institute, The Netherlands), Mohammed Al-Balushi (Department of Microbiology and Immunology, Al Qaboos University, Oman) and Ute Claus (Molecular Life Science Center, Jacobs University Bremen, Germany) for crucial initial experiments with the Y84C/A139C mutants; Tatyana Sandalova and Gengsi Chen (both Science for Life Laboratory, Karolinska Institutet, Sweden) for support with the crystallization; Uschi Wellbrock (Molecular Life Science Center, Jacobs University Bremen, Germany) and Marilyn Aram (Cancer Sciences Unit, University of Southampton, UK) for excellent technical assistance; Henri de la Salle (Inserm, France), Luc van Kaer (Department of Pathology, Microbiology and Immunology, Vanderbilt University, USA) and Edd James (Cancer Sciences, University of Southampton, United Kingdom) for cell lines; Ron Germain (National Institute of Allergy and Infectious Diseases, National Institute of Health, USA) and Kajsa Paulsson (Clinical Genetics, University of Lund, Sweden) for reagents; Martin Zacharias (Department of Physics, Technical University of Munich, Germany) for crucial advice and support with the molecular dynamics simulations; and Tobias Dick (Division of Redox Regulation, German Cancer Research Center, Germany) for a discussion. Anca Tigan (Department of Pharmacology and Toxicology, Veterinary University of Vienna, Austria, Sinan Zhu (Molecular Medicine and Translational Science, Wake Forest School of Medicine, USA) and Eva Weiss (Department of Biology, University of York, UK) provided important data in earlier stages of the work.

Competing interests

The authors declare no competing interests.

Author contributions

Z.H., S.S., T.E., F.M, H.U., A.A. and D.B. designed experiments. Z.H. performed microscopy, cloning and biochemical experiments. H.U. and A.A. crystallized the protein and performed circular dicroism experiments. E.T.A. performed molecular dynamics simulations and thermal denaturation experiments. S.K.S. performed fluorescence anisotropy experiments. L.J. established and performed retroviral transductions. A.V.H. performed in vitro peptide dissociation assays. C.W. and H.H. generated retroviral transduction vectors. F.M. performed the T cell activation assay. Z.H., S.S. and D.B. wrote the manuscript.

Funding

Our work was supported by the Deutsche Forschungsgemeinschaft [grant numbers SP 583/2-3, 7-1, 8-1 to S. Springer, and SPP1230 to H.H.]; the German Federal Ministery of Education and Research [grant 'FoneFA' to H.H.]; the German Academic Exchange Service (to E.T.A.); the Fritz Thyssen Foundation (to Z.H.); the Tönjes Vagt Foundation (to L.J.); Research Commission of the Medical Faculty and the Strategic Research Commission of Heinrich Heine University Duesseldorf (to C.W); Swedish Research Council [grant number 521-2013-3559 to A.A. and H.U.]; Swedish Cancer Society [grant number 130467 to A.A. and H.U.]; and Cancer Research UK [grant number C7056/A11946 to D.S.B., A.V.H. and T.J.E.].

Supplementary material

Supplementary material available online at
http://jcs.biologists.org/lookup/suppl/doi:10.1242/jcs.145334/-/DC1

References

Achour, A., Harris, R. A., Persson, K., Sundbäck, J., Sentman, C. L., Schneider, G., Lindqvist, Y. and Kärre, K. (1999). Murine class I major histocompatibility complex H-2Dd: expression, refolding and crystallization. *Acta Crystallogr. D Biol. Crystallogr.* **55**, 260-262.

Achour, A., Michaëlsson, J., Harris, R. A., Odeberg, J., Grufman, P., Sandberg, J. K., Levitsky, V., Kärre, K., Sandalova, T. and Schneider, G. (2002). A structural basis for LCMV immune evasion: subversion of H-2D(b) and H-2K(b) presentation of gp33 revealed by comparative crystal structure.Analyses. *Immunity* **17**, 757-768.

Achour, A., Michaëlsson, J., Harris, R. A., Ljunggren, H. G., Kärre, K., Schneider, G. and Sandalova, T. (2006). Structural basis of the differential stability and receptor specificity of H-2Db in complex with murine versus human beta2-microglobulin. *J. Mol. Biol.* **356**, 382-396.

Adams, P. D., Afonine, P. V., Bunkóczi, G., Chen, V. B., Davis, I. W., Echols, N., Headd, J. J., Hung, L. W., Kapral, G. J., Grosse-Kunstleve, R. W. et al. (2010). PHENIX: a comprehensive Python-based system for macromolecular structure solution. *Acta Crystallogr. D Biol. Crystallogr.* **66**, 213-221.

Arnold, B., Burgert, H. G., Hamann, U., Hämmerling, G., Kees, U. and Kvist, S. (1984). Cytolytic T cells recognize the two amino-terminal domains of H-2 K antigens in tandem in influenza A infected cells. *Cell* **38**, 79-87.

Bailey, A., van Hateren, A., Elliott, T. and Werner, J. M. (2014). Two polymorphisms facilitate differences in plasticity between two chicken major histocompatibility complex class I proteins. *PLoS ONE* **9**, e89657.

Beerbaum, M., Ballaschk, M., Erdmann, N., Schnick, C., Diehl, A., Uchanska-Ziegler, B., Ziegler, A. and Schmieder, P. (2013). NMR spectroscopy reveals unexpected structural variation at the protein-protein interface in MHC class I molecules. *J. Biomol. NMR* **57**, 167-178.

Bouvier, M. and Wiley, D. C. (1998). Structural characterization of a soluble and partially folded class I major histocompatibility heavy chain/beta 2m heterodimer. *Nat. Struct. Biol.* **5**, 377-384.

Brünger, A. T. (1992). Free R value: a novel statistical quantity for assessing the accuracy of crystal structures. *Nature* **355**, 472-475.

Case, D. A., Cheatham, T. E., 3rd, Darden, T., Gohlke, H., Luo, R., Merz, K. M., Jr, Onufriev, A., Simmerling, C., Wang, B. and Woods, R. J. (2005). The Amber biomolecular simulation programs. *J. Comput. Chem.* **26**, 1668-1688.

Chen, M. and Bouvier, M. (2007). Analysis of interactions in a tapasin/class I complex provides a mechanism for peptide selection. *EMBO J.* **26**, 1681-1690.

Day, P. M., Esquivel, F., Lukszo, J., Bennink, J. R. and Yewdell, J. W. (1995). Effect of TAP on the generation and intracellular trafficking of peptide-receptive major histocompatibility complex class I molecules. *Immunity* **2**, 137-147.

Duan, Y., Wu, C., Chowdhury, S., Lee, M. C., Xiong, G., Zhang, W., Yang, R., Cieplak, P., Luo, R., Lee, T. et al. (2003). A point-charge force field for molecular mechanics simulations of proteins based on condensed-phase quantum mechanical calculations. *J. Comput. Chem.* **24**, 1999-2012.

Ellgaard, L. and Helenius, A. (2001). ER quality control: towards an understanding at the molecular level. *Curr. Opin. Cell Biol.* **13**, 431-437.

Elliott, T., Cerundolo, V., Elvin, J. and Townsend, A. (1991). Peptide-induced conformational change of the class I heavy chain. *Nature* **351**, 402-406.

Emsley, P., Lohkamp, B., Scott, W. G. and Cowtan, K. (2010). Features and development of Coot. *Acta Crystallogr. D Biol. Crystallogr.* **66**, 486-501.

Evans, P. (2006). Scaling and assessment of data quality. *Acta Crystallogr. D Biol. Crystallogr.* **62**, 72-82.

Fahnestock, M. L., Tamir, I., Narhi, L. and Bjorkman, P. J. (1992). Thermal stability comparison of purified empty and peptide-filled forms of a class I MHC molecule. *Science* **258**, 1658-1662.

Fritzsche, S. and Springer, S. (2013). Investigating MHC class I folding and trafficking with pulse-chase experiments. *Mol. Immunol.* **55**, 126-130.

Früh, K., Ahn, K., Djaballah, H., Sempé, P., van Endert, P. M., Tampé, R., Peterson, P. A. and Yang, Y. (1995). A viral inhibitor of peptide transporters for antigen presentation. *Nature* **375**, 415-418.

Garstka, M., Borchert, B., Al-Balushi, M., Praveen, P. V., Kühl, N., Majoul, I., Duden, R. and Springer, S. (2007). Peptide-receptive major histocompatibility complex class I molecules cycle between endoplasmic reticulum and cis-Golgi in wild-type lymphocytes. *J. Biol. Chem.* **282**, 30680-30690.

Garstka, M. A., Fritzsche, S., Lenart, I., Hein, Z., Jankevicius, G., Boyle, L. H., Elliott, T., Trowsdale, J., Antoniou, A. N., Zacharias, M. et al. (2011). Tapasin dependence of major histocompatibility complex class I molecules correlates with their conformational flexibility. *FASEB J.* **25**, 3989-3998.

Grandea, A. G., 3rd, Golovina, T. N., Hamilton, S. E., Sriram, V., Spies, T., Brutkiewicz, R. R., Harty, J. T., Eisenlohr, L. C. and Van Kaer, L. (2000). Impaired assembly yet normal trafficking of MHC class I molecules in Tapasin mutant mice. *Immunity* **13**, 213-222.

Halenius, A., Hauka, S., Dölken, L., Stindt, J., Reinhard, H., Wiek, C., Hanenberg, H., Koszinowski, U. H., Momburg, F. and Hengel, H. (2011). Human cytomegalovirus disrupts the major histocompatibility complex class I peptide-loading complex and inhibits tapasin gene transcription. *J. Virol.* **85**, 3473-3485.

Hämmerling, G. J., Rüsch, E., Tada, N., Kimura, S. and Hämmerling, U. (1982). Localization of allodeterminants on H-2Kb antigens determined with monoclonal antibodies and H-2 mutant mice. *Proc. Natl. Acad. Sci. USA* **79**, 4737-4741.

Hanenberg, H., Xiao, X. L., Dilloo, D., Hashino, K., Kato, I. and Williams, D. A. (1996). Colocalization of retrovirus and target cells on specific fibronectin fragments increases genetic transduction of mammalian cells. *Nat. Med.* **2**, 876-882.

Hanenberg, H., Hashino, K., Konishi, H., Hock, R. A., Kato, I. and Williams, D. A. (1997). Optimization of fibronectin-assisted retroviral gene transfer into human CD34+ hematopoietic cells. *Hum. Gene Ther.* **8**, 2193-2206.

Hee, C. S., Beerbaum, M., Loll, B., Ballaschk, M., Schmieder, P., Uchanska-Ziegler, B. and Ziegler, A. (2013). Dynamics of free versus complexed beta(2)-microglobulin and the evolution of interfaces in MHC class I molecules. *Immunogenetics* **65**, 157-172.

Howarth, M., Williams, A., Tolstrup, A. B. and Elliott, T. (2004). Tapasin enhances MHC class I peptide presentation according to peptide half-life. *Proc. Natl. Acad. Sci. USA* **101**, 11737-11742.

Howe, C., Garstka, M., Al-Balushi, M., Ghanem, E., Antoniou, A. N., Fritzsche, S., Jankevicius, G., Kontouli, N., Schneeweiss, C., Williams, A. et al. (2009). Calreticulin-dependent recycling in the early secretory pathway mediates optimal peptide loading of MHC class I molecules. *EMBO J.* **28**, 3730-3744.

Hsu, V. W., Yuan, L. C., Nuchtern, J. G., Lippincott-Schwartz, J., Hämmerling, G. J. and Klausner, R. D. (1991). A recycling pathway between the endoplasmic reticulum and the Golgi apparatus for retention of unassembled MHC class I molecules. *Nature* **352**, 441-444.

Humphrey, W., Dalke, A. and Schulten, K. (1996). VMD: visual molecular dynamics. *J. Mol. Graph.* **14**, 33-38.

Jorgensen, W. L., Chandrasekhar, J., Madura, J. D., Roger, W. I. and Klein, M. L. (1983). Comparison of simple potential functions for simulating liquid water. *J. Chem. Phys.* **79**, 926-935.

Karttunen, J., Sanderson, S. and Shastri, N. (1992). Detection of rare antigen-presenting cells by the lacZ T-cell activation assay suggests an expression cloning strategy for T-cell antigens. *Proc. Natl. Acad. Sci. USA* **89**, 6020-6024.

Kienast, A., Preuss, M., Winkler, M. and Dick, T. P. (2007). Redox regulation of peptide receptivity of major histocompatibility complex class I molecules by ERp57 and tapasin. *Nat. Immunol.* **8**, 864-872.

Kurimoto, E., Kuroki, K., Yamaguchi, Y., Yagi-Utsumi, M., Igaki, T., Iguchi, T., Maenaka, K. and Kato, K. (2013). Structural and functional mosaic nature of MHC class I molecules in their peptide-free form. *Mol. Immunol.* **55**, 393-399.

Laskowski, R. A., MacArthur, M. W., Moss, D. S. and Thornton, J. M. (1993). PROCHECK: a program to check the stereochemical quality of protein structures. *J. Appl. Cryst.* **26**, 283-291.

Leslie, A. G. W. (1992). Recent changes to the MOSFLM package for processing film and imaging plate data. In *Joint CCP4/ESF-EACBM Newsletter on Protein Crystallography,* No. 26. Warrington: Daresbury Laboratory.

Ljunggren, H. G., Stam, N. J., Ohlén, C., Neefjes, J. J., Höglund, P., Heemels, M. T., Bastin, J., Schumacher, T. N., Townsend, A., Kärre, K. et al. (1990). Empty MHC class I molecules come out in the cold. *Nature* **346**, 476-480.

Mage, M. G., Dolan, M. A., Wang, R., Boyd, L. F., Revilleza, M. J., Robinson, H., Natarajan, K., Myers, N. B., Hansen, T. H. and Margulies, D. H. (2012). The peptide-receptive transition state of MHC class I molecules: insight from structure and molecular dynamics. *J. Immunol.* **189**, 1391-1399.

Mahmutefendić, H., Blagojević, G., Tomaš, M. I., Kučić, N. and Lučin, P. (2011). Segregation of open Major Histocompatibility Class I conformers at the plasma membrane and during endosomal trafficking reveals conformation-based sorting in the endosomal system. *Int. J. Biochem. Cell Biol.* **43**, 504-515.

Mareeva, T., Martinez-Hackert, E. and Sykulev, Y. (2008). How a T cell receptor-like antibody recognizes major histocompatibility complex-bound peptide. *J. Biol. Chem.* **283**, 29053-29059.

McCoy, A. J. (2007). Solving structures of protein complexes by molecular replacement with Phaser. *Acta Crystallogr. D Biol. Crystallogr.* **63**, 32-41.

Morgan, C. S., Holton, J. M., Olafson, B. D., Bjorkman, P. J. and Mayo, S. L. (1997). Circular dichroism determination of class I MHC-peptide equilibrium dissociation constants. *Protein Sci.* **6**, 1771-1773.

Moritz, T., Dutt, P., Xiao, X., Carstanjen, D., Vik, T., Hanenberg, H. and Williams, D. A. (1996). Fibronectin improves transduction of reconstituting hematopoietic stem cells by retroviral vectors: evidence of direct viral binding to chymotryptic carboxy-terminal fragments. *Blood* **88**, 855-862.

Murshudov, G. N., Vagin, A. A. and Dodson, E. J. (1997). Refinement of macromolecular structures by the maximum-likelihood method. *Acta Crystallogr. D Biol. Crystallogr.* **53**, 240-255.

Narzi, D., Becker, C. M., Fiorillo, M. T., Uchanska-Ziegler, B., Ziegler, A. and Böckmann, R. A. (2012). Dynamical characterization of two differentially disease associated MHC class I proteins in complex with viral and self-peptides. *J. Mol. Biol.* **415**, 429-442.

Neefjes, J. J., Smit, L., Gehrmann, M. and Ploegh, H. L. (1992). The fate of the three subunits of major histocompatibility complex class I molecules. *Eur. J. Immunol.* **22**, 1609-1614.

Niman, H. L., Houghten, R. A., Walker, L. E., Reisfeld, R. A., Wilson, I. A., Hogle, J. M. and Lerner, R. A. (1983). Generation of protein-reactive antibodies by short peptides is an event of high frequency: implications for the structural basis of immune recognition. *Proc. Natl. Acad. Sci. USA* **80**, 4949-4953.

Paulsson, K. M., Jevon, M., Wang, J. W., Li, S. and Wang, P. (2006). The double lysine motif of tapasin is a retrieval signal for retention of unstable MHC class I molecules in the endoplasmic reticulum. *J. Immunol.* **176**, 7482-7488.

Peh, C. A., Burrows, S. R., Barnden, M., Khanna, R., Cresswell, P., Moss, D. J. and McCluskey, J. (1998). HLA-B27-restricted antigen presentation in the absence of tapasin reveals polymorphism in mechanisms of HLA class I peptide loading. *Immunity* **8**, 531-542.

Porgador, A., Yewdell, J. W., Deng, Y., Bennink, J. R. and Germain, R. N. (1997). Localization, quantitation, and in situ detection of specific peptide-MHC class I complexes using a monoclonal antibody. *Immunity* **6**, 715-726.

Praveen, P. V., Yaneva, R., Kalbacher, H. and Springer, S. (2010). Tapasin edits peptides on MHC class I molecules by accelerating peptide exchange. *Eur. J. Immunol.* **40**, 214-224.

Purcell, A. W. and Elliott, T. (2008). Molecular machinations of the MHC-I peptide loading complex. *Curr. Opin. Immunol.* **20**, 75-81.

Roder, G., Geironson, L., Darabi, A., Harndahl, M., Schafer-Nielsen, C., Skjødt, K., Buus, S. and Paulsson, K. (2009). The outermost N-terminal region of tapasin facilitates folding of major histocompatibility complex class I. *Eur. J. Immunol.* **39**, 2682-2694.

Ruddock, L. W. and Molinari, M. (2006). N-glycan processing in ER quality control. *J. Cell Sci.* **119**, 4373-4380.

Saini, S. K., Abualrous, E. T., Tigan, A.-S., Covella, K., Wellbrock, U. and Springer, S. (2013). Not all empty MHC class I molecules are molten globules: tryptophan fluorescence reveals a two-step mechanism of thermal denaturation. *Mol. Immunol.* **54**, 386-396.

Sanderson, S. and Shastri, N. (1994). LacZ inducible, antigen/MHC-specific T cell hybrids. *Int. Immunol.* **6**, 369-376.

Schneider, C. A., Rasband, W. S. and Eliceiri, K. W. (2012). NIH Image to ImageJ: 25 years of image analysis. *Nat. Methods* **9**, 671-675.

Serwold, T., Gaw, S. and Shastri, N. (2001). ER aminopeptidases generate a unique pool of peptides for MHC class I molecules. *Nat. Immunol.* **2**, 644-651.

Shastri, N. and Gonzalez, F. (1993). Endogenous generation and presentation of the ovalbumin peptide/Kb complex to T cells. *J. Immunol.* **150**, 2724-2736.

Shields, M. J., Hodgson, W. and Ribaudo, R. K. (1999). Differential association of beta2-microglobulin mutants with MHC class I heavy chains and structural analysis demonstrate allele-specific interactions. *Mol. Immunol.* **36**, 561-573.

Sieker, F., Springer, S. and Zacharias, M. (2007). Comparative molecular dynamics analysis of tapasin-dependent and -independent MHC class I alleles. *Protein Sci.* **16**, 299-308.

Sieker, F., Straatsma, T. P., Springer, S. and Zacharias, M. (2008). Differential tapasin dependence of MHC class I molecules correlates with conformational changes upon peptide dissociation: a molecular dynamics simulation study. *Mol. Immunol.* **45**, 3714-3722.

Springer, S., Döring, K., Skipper, J. C., Townsend, A. R. and Cerundolo, V. (1998). Fast association rates suggest a conformational change in the MHC class I molecule H-2Db upon peptide binding. *Biochemistry* **37**, 3001-3012.

Tiwari, N., Garbi, N., Reinheckel, T., Moldenhauer, G., Hämmerling, G. J. and Momburg, F. (2007). A transporter associated with antigen-processing independent vacuolar pathway for the MHC class I-mediated presentation of endogenous transmembrane proteins. *J. Immunol.* **178**, 7932-7942.

Townsend, A., Ohlén, C., Bastin, J., Ljunggren, H. G., Foster, L. and Kärre, K. (1989). Association of class I major histocompatibility heavy and light chains induced by viral peptides. *Nature* **340**, 443-448.

Townsend, A., Elliott, T., Cerundolo, V., Foster, L., Barber, B. and Tse, A. (1990). Assembly of MHC class I molecules analyzed in vitro. *Cell* **62**, 285-295.

Van Hateren, A., James, E., Bailey, A., Phillips, A., Dalchau, N. and Elliott, T. (2010). The cell biology of major histocompatibility complex class I assembly: towards a molecular understanding. *Tissue Antigens* **76**, 259-275.

Van Kaer, L., Ashton-Rickardt, P. G., Ploegh, H. L. and Tonegawa, S. (1992). TAP1 mutant mice are deficient in antigen presentation, surface class I molecules, and CD4-8+ T cells. *Cell* **71**, 1205-1214.

Velloso, L. M., Michaëlsson, J., Ljunggren, H. G., Schneider, G. and Achour, A. (2004). Determination of structural principles underlying three different modes of lymphocytic choriomeningitis virus escape from CTL recognition. *J. Immunol.* **172**, 5504-5511.

Journal of Cell Science

Wang, H., Capps, G. G., Robinson, B. E. and Zúñiga, M. C. (1994). Ab initio association with beta 2-microglobulin during biosynthesis of the H-2Ld class I major histocompatibility complex heavy chain promotes proper disulfide bond formation and stable peptide binding. *J. Biol. Chem.* **269**, 22276-22281.

Wearsch, P. A. and Cresswell, P. (2007). Selective loading of high-affinity peptides onto major histocompatibility complex class I molecules by the tapasin-ERp57 heterodimer. *Nat. Immunol.* **8**, 873-881.

Wearsch, P. A. and Cresswell, P. (2008). The quality control of MHC class I peptide loading. *Curr. Opin. Cell Biol.* **20**, 624-631.

Williams, A. P., Peh, C. A., Purcell, A. W., McCluskey, J. and Elliott, T. (2002). Optimization of the MHC class I peptide cargo is dependent on tapasin. *Immunity* **16**, 509-520.

Wright, C. A., Kozik, P., Zacharias, M. and Springer, S. (2004). Tapasin and other chaperones: models of the MHC class I loading complex. *Biol. Chem.* **385**, 763-778.

Zacharias, M. and Springer, S. (2004). Conformational flexibility of the MHC class I alpha1-alpha2 domain in peptide bound and free states: a molecular dynamics simulation study. *Biophys. J.* **87**, 2203-2214.

Zagorac, G. B., Mahmutefendić, H., Tomaš, M. I., Kučić, N., Le Bouteiller, P. and Lučin, P. (2012). Early endosomal rerouting of major histocompatibility class I conformers. *J. Cell. Physiol.* **227**, 2953-2964.

Zhang, W., Wearsch, P. A., Zhu, Y., Leonhardt, R. M. and Cresswell, P. (2011). A role for UDP-glucose glycoprotein glucosyltransferase in expression and quality control of MHC class I molecules. *Proc. Natl. Acad. Sci. USA* **108**, 4956-4961.

Zimmer, J., Donato, L., Hanau, D., Cazenave, J. P., Moretta, A., Tongio, M. M. and de la Salle, H. (1999). Inefficient protection of human TAP-deficient fibroblasts from autologous NK cell-mediated lysis by cytokines inducing HLA class I expression. *Eur. J. Immunol.* **29**, 1286-1291.

Supplementary information

Peptide-independent stabilization of MHC class I molecules breaches cellular quality control

Zeynep Hein[1], Hannes Uchtenhagen[2], Esam Tolba Abualrous[1], Sunil Kumar Saini[1], Linda Janßen[1], Andy Van Hateren[3], Constanze Wiek[4], Helmut Hanenberg[4], Frank Momburg[5], Adnane Achour[2], Tim Elliott[3], Sebastian Springer[1], Denise Boulanger[3]

[1]Molecular Life Science Center, Jacobs University Bremen, Germany.

[2]Science for Life Laboratory, Department of Medicine Solna, Karolinska Institutet, Stockholm, Sweden.

[3]Cancer Sciences Unit, Faculty of Medicine, University of Southampton, Southampton, Hampshire, United Kingdom.

[4]Department of Otorhinolaryngology, Heinrich-Heine-University Düsseldorf, Düsseldorf, Germany.

[5]Translational Immunology Research Unit, German Cancer Research Center, Heidelberg, Germany.

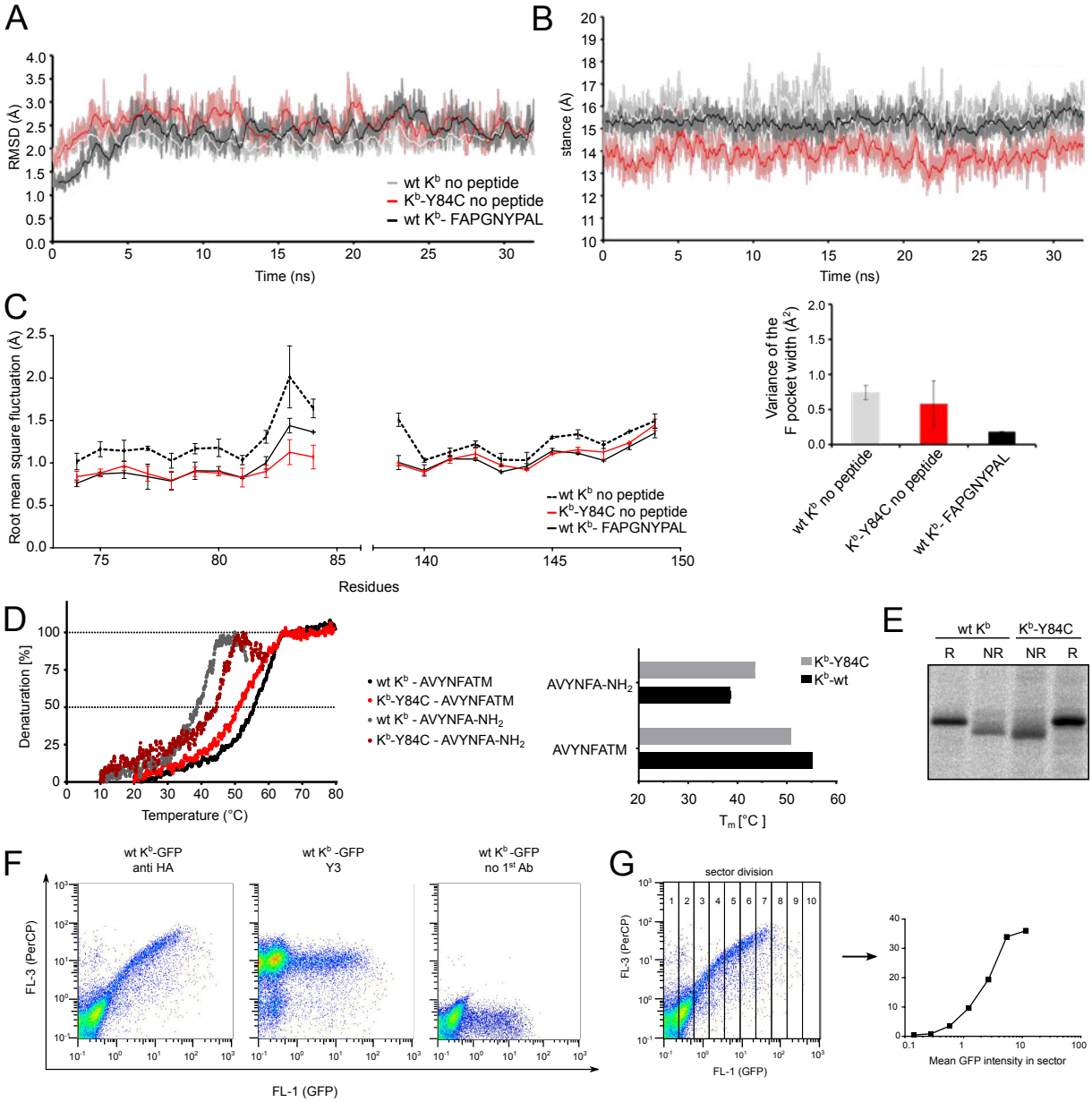

SUPPLEMENTARY FIGURE S1. A-C. In K^b-Y84C, the mobility of the polypeptide backbone in the F pocket region is restrained, whereas the overall backbone mobilities of wild type K^b and K^b-Y84C are very similar. Data from a 32 ns molecular dynamics simulation following 8 ns equilibration; see also Figure 1B, C, D. **A**. The mobilities of the polypeptide backbones of the three K^b proteins (wild type K^b without peptide, wild type K^b in complex with FAPGNYPAL, and K^b-Y84C without peptide) are similar. Root mean square deviations (RMSD, calculated relative to the starting crystal structure) of the α carbons of the entire polypeptide backbone of the K^b proteins during the simulations. **B**. The width of the F pocket is restrained in K^b-Y84C. Top: F pocket width (measured as the distance between the centers of mass of the α carbons of residues 73 to 84 and the α carbons of residues 139 to 150) plotted against simulation time. Bottom: Variance of the F pocket widths over the course of the simulation. **C**. Root mean square fluctuations (RMSF) of the α carbons of the residues in the direct vicinity of residues 84 (left) and 139 (right), the site of the C84-C139 disulfide bond in K^b-Y84C. **D**. Stability of K^b-peptide complexes determined by circular dichroism. Complexes of K^b with murine β_2m and with the indicated peptides were prepared by in vitro folding, subjected to heat denaturation, and circular dichroism was recorded at 218 nm. The transition midpoint (melting temperature, Tm) is the 50% line intersection of the curves and depicted as a bar chart on the right panel. AVYNFA-NH_2 has a C-terminal amide to prevent repulsion of the truncated carboxyl terminus in the binding groove. **E**. The additional disulfide bond of K^b-Y84C forms in vivo. COS cells were transiently transfected with K^b heavy chains containing an N-terminal HA tag, radioactively labeled with [^{35}S] methionine, and lysed. 20 mM N-ethylmaleimide was added to the lysates to block free thiol groups. K^b molecules were immunoprecipitated with anti-HA MAb, and immunoisolates were denatured (lanes NR) or denatured and reduced (lanes R) and resolved on a 6-16% SDS-polyacrylamide gel. **F**. Quantification of K^b expression at the cell surface. Flow cytometry plots. K^b GFP was expressed in BL/6 fibroblasts. Cells were stained with monoclonal antibodies to the N-terminal HA (influenza hemagglutinin) tag and subsequently with PerCP-conjugated anti-mouse secondary antibody, and then the cells were analyzed by flow cytometry. Plots show for each cell the surface levels of K^b molecules (y axis) vs. the GFP signal, i.e., the total cellular amount of K^b GFP (x axis). **G**. Quantification of flow cytometry data. Flow cytometry plots were divided into ten numbered sectors (left panel). For sectors 1 to 8 of each sample, the mean intensity of surface staining (mean y) was calculated and plotted against the GFP mean fluorescence intensity (mean x) (right panel). This way of quantification was used in Figures 3 ABC,4A, and S2E.

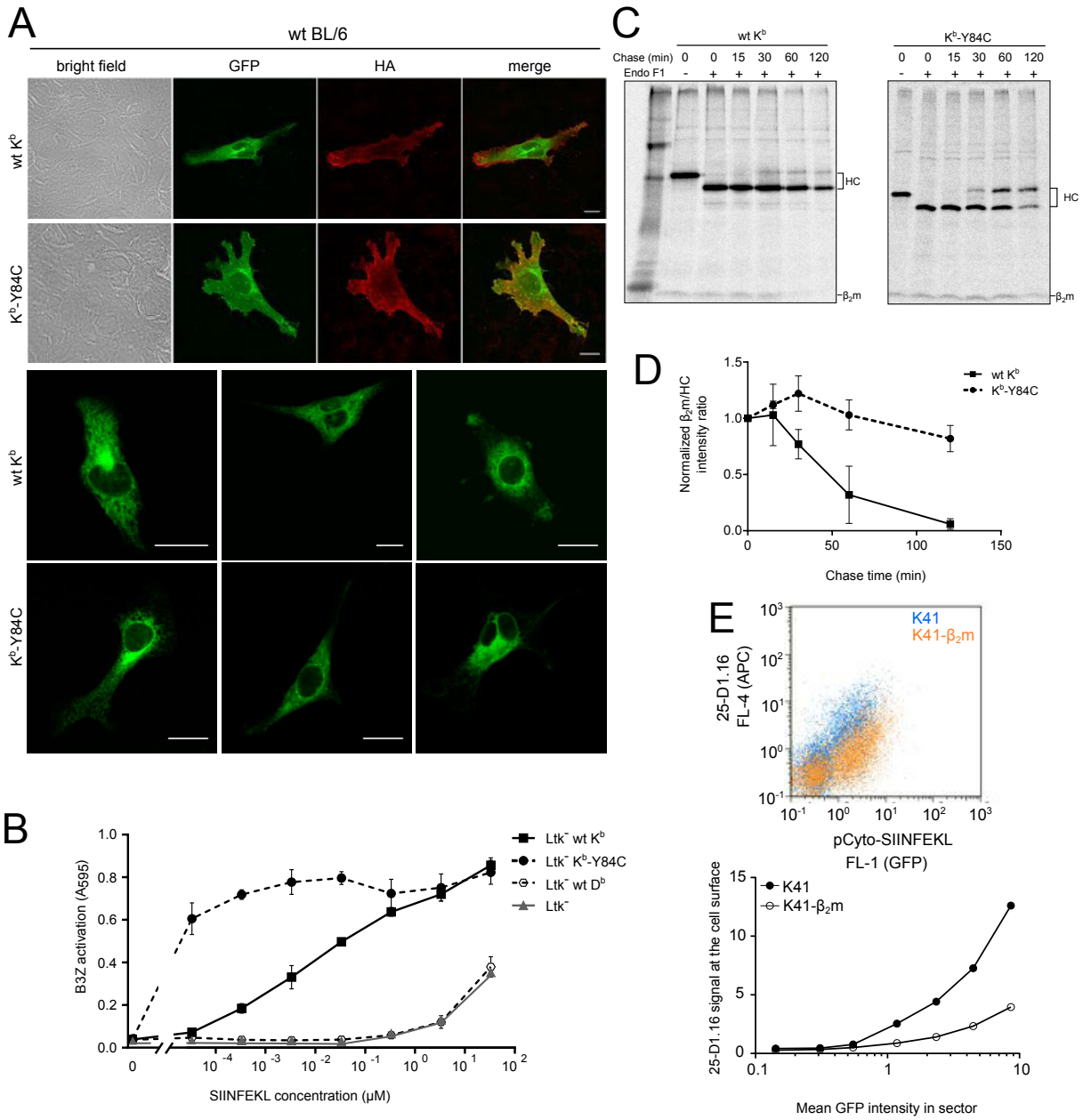

SUPPLEMENTARY FIGURE S2. A.K^b-GFP constructs are expressed at the cell surface in wild type cells. Wild type BL/6 fibroblasts were transfected with HA-K^b-GFP constructs (green; upper and lower panel), and surface K^b molecules were detected by staining with an anti-HA MAb (red; upper panel only). **B**. K^b-Y84C is highly efficient in presenting peptide to T cells. Ltk- cells (H-2k) were transiently transfected with MHC-I heavy chains as indicated, incubated with indicated amounts of SIINFEKL peptide, and cocultured with B3Z cells. T cell activity was measured by a β galactosidase assay. The mean fluorescence intensity levels of transiently transfected cells were: untransfected, 112 and 125 (with K10-56 (K^b) and B22.249 (D^b) antibodies, respectively; see materials and methods); wild type D^b, 2682 (B22.249); wild type K^b, 703 (K10-56); K^b-Y84C, 650 (K10-56). **C**. K^b-Y84C has an increased affinity to β_2m.Image of the entire SDS-PAGE gel of a pulse chase experiment performed in TAP deficient BL/6 fibroblasts, similar to that shown in Figure 5 (center panel), showing the band for co-immunoprecipitated β_2m at the bottom. **D**. Quantification of the β_2m and K^b heavy chain bands. The errors are ± SEM, n=2. **E**. Overexpression of β_2m impairs high affinity peptide selection in wild type cells. K41 fibroblasts were stably transduced with human β_2m. Wild type and β_2m-overexpressing cells were infected with lentiviruses coding for MSIINFEKL-IRES-GFP gene product (pCyto-SIINFEKL). Surface K^b-SIINFEKL complexes were detected by staining non-permeabilized cells by 25-D1.16 antibody. Dot plots (top) were quantified as explained in Fig.S1G and depicted in a linear graph (bottom).

Supplementary Table 1. Statistics of diffraction data and structure refinement

	K[b]-Y84C/AVYNFATM
Statistics of diffraction data	
PDB ID	4HS3
Wavelength (Å)[a]	0.87260
Resolution (Å)	40.9-2.1 (2.2-2.1)
Space group	$P2_12_12_1$
Unit-cell parameters (Å)	$a = 45.6$ $b = 90.6$, $c = 137.4$
No. of observed reflections	111070 (14465)
No. of unique reflections	32975 (4754)
Redundancy	3.4 (3.0)
Completeness (%)	97 (98)
R_{merge}[b] (%)	13.0 (60.0)
‹I/σ(I)›	7.8 (2.6)
Statistics of refinement and structure model	
No. of molecules in ASU	1
R_{cryst}[c] (%)	18.0
R_{free}[d] (%)	22.9
Number of atoms	
protein	3154
water	418
ligand	13
RMSD from ideal geometry	
bond lengths (Å)	0.008
bond angles (°)	1.07
Average B factor (Å^2)[e]	
Protein	24.20
Solvent	33.10
Ramachandran plot (%)	
Most favored regions	92.1
Allowed regions	7.6
Generously allowed regions	0.3
Disallowed regions	0.0

[a] Number in parentheses indicate the outer-resolution shell.

[b] $R_{merge} = \sum_{hkl} \sum_i \left| I_i(hkl) - \langle I(hkl) \rangle \right| / \sum_{hkl} \sum_i I_i(hkl)$, where $I_i(hkl)$ is the ith observation of reflection hkl and ‹I (hkl)› is the weighted average intensity for all observations i of reflection hkl.

[c] $R_{cryst} = \sum_{hkl} |F_{obs} - F_{calc}| / \Sigma_{hkl} |F_{obs}|$, where $|F_{obs}|$ and $|F_{calc}|$ are the observed and calculated structure factor amplitudes of a particular reflection and the summation is over 95% of the reflections in the specified resolution range. The remaining 5% of the reflections were randomly selected (test set) before the structure refinement and not included in the structure refinement.

[d] R_{free} was calculated for the test set using the same equation as for R_{cryst}.

Supplementary Table 2: Comparison of wild type K_b/gp34 and K^b-Y84C/gp34 structures.
Calculated root mean square deviation (RMSD) of the Cα atoms between the indicated portions of the structures of wild type K^b/gp34 (PDB 1S7S, Fig. 2) and K^b-Y84C/gp34 (PDB 3ROO, Fig. 2) or wild type K^b/gp33 (PDB 1S7Q).
The RMSD values between the two wild-type structures (wild type K^b/gp34 and wild type K^b/gp33) are included as a comparison for two structures that are essentially identical.
Resolutions are: K^b-Y84C/gp34 = 2.1 Å; wild type K^b/gp34 = 2.0 Å; wild type Kb/gp33 = 2.0 Å.

	RMSD (Å) between wild type K^b and :	
	K^b-Y84C/gp34	wild type K^b/gp33
entire complex	0.45	0.43
heavy chain only	0.47	0.44
β_2m only	0.24	0.22
peptide only	0.12	0.15
peptide binding cleft (2-176) only	0.32	0.26